Report Documentation Page

Form Approved
OMB No. 0704-0188

1. REPORT DATE	2. REPORT TYPE	3. DATES COVERED
JUN 2012		**00-00-2012 to 00-00-2012**

4. TITLE AND SUBTITLE	5a. CONTRACT NUMBER
An Investigation of Chitosan for Sorption of Radionuclides.	5b. GRANT NUMBER
	5c. PROGRAM ELEMENT NUMBER
6. AUTHOR(S)	5d. PROJECT NUMBER
	5e. TASK NUMBER
	5f. WORK UNIT NUMBER
7. PERFORMING ORGANIZATION NAME(S) AND ADDRESS(ES) **Oregon State University,104 Kerr Administration Building ,Corvallis,OR,97331**	8. PERFORMING ORGANIZATION REPORT NUMBER
9. SPONSORING/MONITORING AGENCY NAME(S) AND ADDRESS(ES)	10. SPONSOR/MONITOR'S ACRONYM(S)
	11. SPONSOR/MONITOR'S REPORT NUMBER(S)

12. DISTRIBUTION/AVAILABILITY STATEMENT
Approved for public release; distribution unlimited

13. SUPPLEMENTARY NOTES

14. ABSTRACT
Chitosan is a biopolymer resulting from the deacetylation of chitin, the second most abundant biopolymer in nature. Chitosan has been successfully used in systems to remove metal ions and other pollutants from wastewater. Chitosan has shown promise as a sorbent for radionuclides in some aqueous waste streams.

15. SUBJECT TERMS

16. SECURITY CLASSIFICATION OF:			17. LIMITATION OF ABSTRACT	18. NUMBER OF PAGES	19a. NAME OF RESPONSIBLE PERSON
a. REPORT	b. ABSTRACT	c. THIS PAGE			
unclassified	**unclassified**	**unclassified**	**Same as Report (SAR)**	**100**	

AN ABSTRACT OF THE THESIS OF

Vanessa E. Holfeltz for the degree of Master of Science in
Radiation Health Physics presented on June 5, 2012.
Title: An Investigation of Chitosan for Sorption of Radionuclides.

Abstract approved: _____

Alena Paulenova

Chitosan is a biopolymer resulting from the deacetylation of chitin, the second most abundant biopolymer in nature. Chitosan has been successfully used in systems to remove metal ions and other pollutants from wastewater. Chitosan has shown promise as a sorbent for radionuclides in some aqueous waste streams.

The sorption of these radionuclides by chitosan is studied to determine if chitosan could be used as a sorbent for aqueous waste streams containing these metals. The effect of various experimental conditions including sorbent particle size, agitation rate, hydration, temperature, pH, metal concentration and sorbent concentration are examined in this study. Results showed that sorption depends on the availability of access sites, controlled by the specific surface area of the sorbent. Sorption was observed to decrease with increasing temperature.

The sorption isotherms and kinetics for Co(II), Eu(III) and U(VI) sorption onto chitosan were determined experimentally by batch sorption. Isotherms were fitted using the Langmuir and Freundlich models. Kinetics were modeled using the pseudo-first order, pseudo-second order, Elovich, and intraparticle diffusion models in order to determine possible rate-limiting steps. Most data were well described by the pseudo-second order and Elovich models. Multi-linearity was observed in the intraparticle diffusion model. The sorption capacity of the metals on chitosan was found to follow the order Co < Eu < U.

An Investigation of Chitosan for Sorption of Radionuclides

by

Vanessa E. Holfeltz

A THESIS

submitted to

Oregon State University

in partial fulfillment of
the requirements for the
degree of

Master of Science

Presented June 5, 2012
Commencement June 2013

Master of Science thesis of Vanessa E. Holfeltz presented on June 5, 2012.

APPROVED:

Major Professor, representing Radiation Health Physics

Head of the Department of Nuclear Engineering and Radiation Health Physics

Dean of the Graduate School

I understand that my thesis will become part of the permanent collection of Oregon State University libraries. My signature below authorizes release of my thesis to any reader upon request.

Vanessa E. Holfeltz, Author

ACKNOWLEDGMENTS

I would like to express my appreciation and thanks to my advisor, Dr. Alena Paulenova, for guidance and support throughout the project presented in this work. I also wish to thank my committee members, Dr. Kathryn Higley, Dr. Gregory Rorrer and Dr. Laurel Kincl.

I also wish to thank the radiochemistry research group, and especially Alex, Joey, and Martin, for their helpful discussions and guidance.

I also wish to acknowledge Dr. Scott Menn and Shaun Bromagen, for their assistance in obtaining materials throughout this project.

Financial support for this project was provided by the US Department of Army (DoA) award W911NF-10-1-0325. The contents are solely the responsibility of the authors and do not necessarily represent the official views of the OBEI or DoA.

TABLE OF CONTENTS

TABLE OF CONTENTS (Continued)

Page

LIST OF FIGURES

LIST OF FIGURES (Continued)

Figure Page

LIST OF TABLES

AN INVESTIGATION OF CHITOSAN FOR SORPTION OF RADIONUCLIDES

1 Introduction

Many modern industries, including the nuclear industry, result in wastewaters and effluents containing various pollutants. Among the pollutants are various metals which may pose toxicity risks to biota after their release into the environment, where they may be bioconcentrated with increasing trophic level. The removal of toxic metals from wastewaters prevents their release into the biosphere. There are various methods and technologies used for decontamination of industrial wastewater, including chemical precipitation, electrochemical methods, filtration, ion exchange and adsorption [10, 13, 56].

The nuclear technologies, including both nuclear energy and nuclear medicine applications, produce aqueous waste containing various radioactive metals. The treatment and processing of these wastes into more stable chemical and physical form is necessary to prevent the release of the radionuclides into the environment. An ideal treatment method will immobilize and concentrate the radionuclides; result in a minimal amount of secondary radioactive waste; result in secondary waste that is easily disposed of; and be cost effective. The International Atomic Energy Agency (IAEA) has identified several areas of so-called "problem waste", including aqueous waste and spent ion exchange resins, and have expressed the need to develop effective technologies to treat these wastes for final disposal [16]. Among the identified problem wastes are aqueous wastes unsuitable for standard treatment methods, such as those containing organic substances. The proposed method is to treat the wastes to make them amenable to treatment by the standard methods. An alternate method would be to use a new technology capable of treating both in one step.

Chitosan, a biopolymer derived of chitin, has been used as a biosorbent for a wide variety metals in aqueous solution. Chitin is very abundant in the biosphere,

notably in the shells of arthopods, and is readily available a byproduct of the seafood industry. Chitosan is readily chemically modified to a form suitable for use large systems, and has been shown to sorb a wide variety of pollutants, including metal ions, organic dyes, phenols, nitrates, and humic substances [8]. Additionally, chitosan has been found to readily form a covalent bond with carboxylic acids such as EDTA and DTPA [26]. These are commonly used as chelators for radionuclides in the nuclear industry, and have required pre-processing by photodegradation in some "problem wastes" before the radionuclides could be removed by standard methods [16]. The potential for chitosan to sorb both the carboxylic acids and the radionuclide may result in a more efficient one-step process.

Another attractive feature of chitosan as a sorbent for radionuclides concerns its disposal. Currently, organic ion exchange resins used for treatment of radio-waste are either completely immobilized or the organic component is destroyed. Chitosan, like chitin, is easily biodegradable, and can be completely biodegraded before final deposition. Additionally, chitosan follows the "CHON principle", an approach being applied in development of methods for irradiated nuclear fuel reprocessing that utilizes materials consisting only of **c**arbon, **h**ydrogen, **o**xygen and **n**itrogen, as such materials can be easily incinerated thereby resulting in less secondary waste.

The design of a sorbent system based on chitosan requires knowledge of the kinetics and sorption capacity of the system for the target sorbates, among other factors. In this work, the removal of Co(II), Eu(III) and U(VI) (as UO_2^{2+}) from aqueous solutions by chitosan has been investigated. Equilibrium and kinetic experiments have been performed using chitosan of different composition and particle size, and in solution at various pH, temperature, and metal concentration. The sorption capacity for these metals has been determined by the Langmuir and Freundlich isotherms. Various kinetic models have been used to determine the likely rate-controlling steps of sorption.

Chapter 2 presents a review of the characteristics and applications of chitosan, biosorption, and the principles of sorption equilibrium and kinetics modeling. Chapter

3 describes the experimental and analytical methods used in this work. The experimental results and discussion are presented in Chapter 4, and Chapter 5 presents the conclusions of this work.

2 Background

Chitosan has been investigated for use as a biosorbent for a number of aqueous pollutants, including metallic species and organic dyes. The performance of chitosan as a sorbent for aqueous pollutants will depend on physicochemical properties of the chitosan itself and the mechanism of sorption. The performance of a sorbent is evaluated by determining its capacity and kinetics by application of models. The kinetics and capacity of a sorbent must be established before it can be successfully applied on an industrial scale.

2.1 Chitosan

Chitin, the parent material of chitosan, is the second most abundant biopolymer in nature (after cellulose), and is found in a variety of organisms, including crustaceans, insects, cephalopods, and fungi. In arthopods, it is primarily found in the exoskeleton, where it can comprise up to 80% of the organism [54]. Chitin was first discovered in 1811 by Henri Braconnot, in his course of study of fungi. Odier discovered the presence of chitin in insects in 1823, and gave chitin its name, from the Greek $\chi\iota\tau\omega\nu$ (tunic; envelope). Chitin was not described as a polysaccharide of glucosamine until 1946, by Purchase and Braun [54]. Since then, the study of chitin and chitosan has grown exponentially.

2.1.1 Physicochemical properties

Chitin is a polymer consisting primarily of monomer units of 2-acetamido-2-deoxy-D-glucose-(N-acetylglucosamine), as shown in Figure 2.1. Chitin is highly crystalline, hydrophobic and insoluble in water and most organic solvents [75], although it is soluble in concentrated mineral acids [54]. Chitin becomes soluble as it is deacetylated; when more than 50% of the acetyl groups are removed, it becomes soluble in acidic solution. The solubility of chitin in acidic solution has been used to define and distinguish chitin from chitosan, with chitosan defined as chitin that has been deacety-

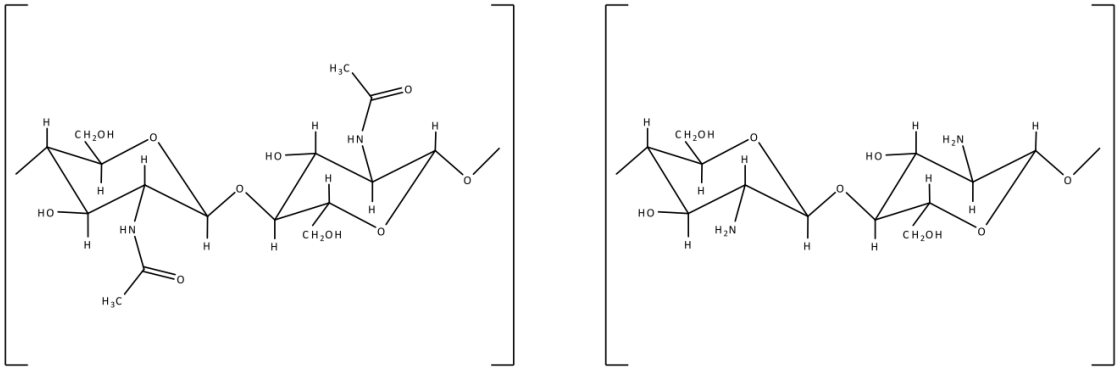

Figure 2.1: Structure of the chitin (left) and chitosan (right) monomer units.

lated to the point that it is soluble in dilute acetic acid [54, 75]. An alternate definition of chitosan is when more than approximately 60% of the monomer units are deacetylated and the polymer is acid soluble [84]. A strict nomenclature for the difference between chitin and chitosan has not been rigorously applied [72]. Chitosan becomes soluble in acidic media due to protonation of its amine groups; this also results in chitosan becoming polycationic in solution [75].

Chitosan is primarily produced by the deacetylation of chitin. On the industrial scale this is accomplished by basic hydrolysis of the acetyl group using sodium hydroxide [21, 72]. The basic hydrolysis process is used preferentially to an acid hydrolysis process, as acid hydrolysis results in greater degradation and depolymerization [54]. Basic hydrolysis of chitin is usually performed in strong sodium hydroxide (40–100%) at elevated temperature (above 100°C) for several hours. Longer treatment times result in a final product with more acetyl groups removed, but also with a lower molecular weight [54]. In the deacetylation process, acetyl groups are removed from the polymers randomly, resulting in a final polymer that has a random distribution of acetylglucosamine and glucosamine units.

Chitosan is primarily characterized by three properties: its degree of acetylation, crystallinity, and the polymer molecular weight. These properties will determine how chitosan behaves in solution, as well as determining its biological and physicochemical properties [84].

Perhaps the most important of these parameters, especially for metal sorption, is the degree of acetylation (DA), which is defined as the molar fraction of acetylated monomer units. Chitosan is alternately characterized in some works by its degree of deacetylation (DDA), defined as the molar fraction of de-acetylated monomer units. Note that the relationships $\text{DA} = 1 - \text{DDA}$ and $\text{DDA} = 1 - \text{DA}$ automatically hold. Both DA and DDA are expressed as percentages. The DDA of chitosan determines how many amine groups are present; it is generally accepted that amine groups are the site of chitosan-metal interactions. The DDA actually provides an upper bound on the number of amine groups available for complexation: some amine groups will be unavailable due to physical inaccessibility or involvement in inter- or intra- molecular hydrogen bonding. The pK_a of chitosan depends on the degree of deacetylation, and has been published to be from 6.1 to 7 [84]. The intrinsic pK, pK_0, also depends on DDA and has been reported to range from 6.46 to 7.32 [79].

Several methods have been used to determine the DDA of chitosan, including ^{1}H NMR, ^{13}C NMR, FTIR, UV spectrophotometry, NIR spectroscopy, potentiometry and colorimetric methods [7, 38, 77]. Of these, ^{1}H NMR has been found to be simple, rapid, and more precise than many of the other methods [47]. Kasaai reviewed the various NMR methods for determination of DDA on chitosan, and concluded that ^{1}H NMR is the most sensitive and accurate NMR method, although solid state NMR methods offer certain advantages regarding sample preparation and all of the NMR methods are sensitive to interference from impurities and moisture [39]. Balázs and Sipos determined that for the potentiometric method to yield results in agreement with those of ^{1}H NMR, certain conditions must apply, such as having DDA over 75% and knowing precisely the moisture and ash content of the samples [5]. Near infrared (NIR) spectroscopy has been introduced as a rapid method for N-acetylation determination; however, this method requires calibration using a chitosan standard with DDA determined by another method, such as ^{1}H NMR [71]. Tan et al. found a good correlation between first-derivative UV-spectrophotometry and ^{1}H NMR results, and advocate the use of this method [85]. This method requires a calibration curve us-

ing N-acetyl-D-glucosamine, but is more robust to protein contamination than NMR spectroscopy. Determination of DDA by FTIR is dependent upon the choice of absorption bands compared, the choice of baseline subtraction, and requires a calibration curve made by a chitosan of known DDA [81]. Kahn et al. performed a comparison of varisou methods of DDA determination, and determined that the DDA value obtained is highly dependent upon the analysis method used [41].

The polymer weight (alternatively, the molecular weight) of chitosan depends largely on the method of production, i.e., the method and conditions of deacetylation. The polymer weight can be found by several methods, including size exclusion chromatography, static light scattering, and viscometry [22, 64, 79, 84]. Viscometry is one of the simpler and more popular methods to determine chitosan PW. Chitosan is available commercially with PW from 10,000 to 1,000,000 daltons [60].

Polymer weight (PW) can determine the solubility of chitosan in solution, as the solubility decreases with increasing PW. Park et al. found the tensile strength of chitosan films increased with the PW of the chitosan used in the films [62]. Cárdenas et al. report that the PW of chitosan influences the bacteriological properties of chitosan- and chitosan-composite films [11]. Zhang and Neau found that the PW of chitosan had a slower degradation rate in the presence of an enzyme [96]. The PW of chitosan has also been found to have an effect on the performance of chitosan used as a coagulant-flocculant in waste water treatment [2].

Crystallinity has been found to have an effect on metal sorption. Piron et al. found that the crystallinity of samples of chitosan controlled the sorption rate and total uptake of uranyl on chitosan, concluding that sorption was only possible in the amorphous domains and not in the crystalline domains [64]. The crystallinity of the polymer can also control the accessibility of the amine groups [21]. The crystallinity of chitosan is determined by x-ray diffraction (XRD) by analysis of the (two superimposed) peaks at $2\theta = 20^\circ$ [37]. Zhang et al. found a linear decrease of the crystallinity index (determined by XRD) with increasing DDA, suggesting that XRD may be used to determine the DDA of some samples. Jaworska et al. found that dissolving and

re-drying chitosan resulted in a decrease in crystallinity, and that dissolving followed by freeze-drying resulted in an even greater decrease in crystallinity [37]. These authors also found a dependence of the crystallinity index on the source of chitosan; in increasing crystallinity: fungal chitosan < squid chitosan < shrimp chitosan.

Chitin has been observed in three polymorphic forms, categorized by the arrangement of the polymer chains: α-chitin (anti-parallel chains), β-chitin (parallel chains) and γ-chitin (mixed arrangement) [37]. The arrangement of the chains is found to depend on the origin of the chitin; for example, α-chitin is found in the cuticle of arthopods and β-chitin is found in the pen and cuticle of squid. α-chitin is by far the most abundant. In α-chitin, sheets are formed by intermolecular hydrogen bonding in parallel chains. Interchain hydrogen boding occurs between sheets in different directions. There are also intermolecular hydrogen bonding between CH_2OH groups, which is believed to be the cause for the lack of swelling of α-chitin in water [37, 58]. In β-chitin, hydrogen bonding occurs only within sheets, not between sheets as in α-chitin. This is thought to be responsible for the swelling of β-chitin, as water (or other guest molecules) can be included between the sheets. γ- chitin is considered to be a mixture of the α- and β- configurations [58, 75].

2.1.2 Chitosan modification and derivatives

Chitosan has been modified, both physically and chemically, to alter its properties to suit various applications.

Chitosan has been physically modified in a variety of ways, resulting in conditioned forms such as powders, nanoparticles, gel beads, gels, fibers, and sponge [21]. Such conditioning of "raw" chitosan can result in better performance. Guibal et al. produced microcrystalline chitosan by dissolution in acetic acid, precipitation and gentle drying, which resulted in a decrease in crystallinity and PW, which had favorable sorption for uranyl [24]. Hsien and Rorrer created highly porous chitosan gel beads by using freeze-drying to maintain the porous structure of the beads [31]. Gel beads are formed by casting an aqueous solution (chitosan dissolved in acetic acid)

into a NaOH or methanol-NaOH bath to precipitate the beads, followed by drying or freeze-drying [22, 82]. Membranes have been prepared by many authors by casting a solution of chitosan in acetic acid onto a surface and letting the solvent evaporate [21]. Pillai has reviewed the formation of chitosan into fibers, which has been done with a wide variety of solvent systems and co-materials [63].

Chemical modification is usually done in order to improve the sorption properties for a particular sorbate or to prevent dissolution of the polymer [21]. Chitosan is not suitable for use in acidic conditions, as the polymer dissolves. To inhibit the dissolution, chitosan can be cross-linked. Common cross-linkers are tripolyphosphate, glutaraldehyde, epichlorohydrin and ethylene glycol diglycidyl ether [49]. Crosslinking has been found to decrease sorption capacity in some cases, as well as having effects on some of the physical properties of chitosan, such as a reduction in the crushing strength [30]. Many of the cross linking procedures that have been used take place at amine groups, rendering them unavailable as sites for metal complexation, which may result in a decrease in sorption capacity due to the decrease in sorption sites (amine groups) [21].

Grafting functional groups can impart new functionality to chitosan, by increasing the density of sorption sites or by increasing the selectivity for a target sorbate [21]. Many different functional groups have been grafted onto chitosan, with grafting occurring at either the amine or hydroxyl groups. The addition of functional groups has been observed to change the pH at which certain metals are adsorbed; for example, Inoue et al. found that copper sorption onto EDTA- and DTPA-grafted chitosan occurs at lower pH than on unmodified chitosan [33]. Valenta et al. found that hydrogels made of EDTA-chitsoan were resistant to bacterial growth [88]. Nishi et al. found that alkaline earth metals, which are typically very poorly sorbed by chitin and chitosan, were sorbable by phosphorylated chitin [57]. Sakaguchi et al. used phosphorylated chitin and chitosan for sorption of selected alkalkine earth, transition metals, and uranyl, and found good sorption capacity for uranyl [78]. Several reviews of chitosan derivatives have been recently published [8, 21, 75, 89].

Table 2.1: Select applications of chitosan. *From [72, 75].*

Agriculture	Seed coating, frost protection
	time release fertilizers
Water and	Flocculant for water treatment
waste treatment	Removal of metal ions
	Removal of dyes
Food	Protective coating for fruits
	Thickener and stabilizer
Biomedical	Hemostatic bandages, wound dressings
	Artificial skin
	Controlled release pharmaceuticals

2.1.3 Chitosan applications

Chitosan has found applications in a wide range of fields, including agriculture, water treatment, biomedical and pharmaceutical, food, cosmetics and textile industries. A summary of select applications of chitosan are presented in Table 2.1.

2.2 Biosorption

The term *biosorption* is used to describe the accumulation of metal ions (or other contaminants and pollutants) onto material of biological origin. The biomaterial may be a living or dead organism; however, generally the term *bioaccumulation* is applied to the case of a live organism, and *biosorption* is reserved for the case of accumulation onto non-living organisms [13]. Interest in biosorption dates to at least the 1980s, when it was recognized as a possible cost-effective solution to recover metal ions (and other contaminants) from industrial aqueous waste streams or for the recovery of valuable metals from natural waters [78, 87]. Biomaterials of many origins have been identified as candidates for the removal of various candidates, including (but not limited to) fungal biomass, seaweed, peat, eggshell, spent brewery yeast, marine algae, silk, wool, feathers, alginate and chitn/chitosan [3, 13, 34, 35, 76].

Anthropogenic environmental pollution has resulted in the release of many metallic species into the biosphere, many of them toxic. Once in the biosphere, the

metals cycle between biotic and abiotic components, where they can be concentrated in particular biota, resulting in potential toxicity [13, 91]. Remediation of such toxic metals is accomplished only when the metals are sufficiently immobilized or removed from the environment. By appropriate immobilization, the metals can be made biounavailable to biota in the system or even fully recovered and removed, thus reducing the toxicity to the biosphere [91].

Research in biosorption has primarily been focused on the removal of metal ions, including transition metals, heavy metals, uranium and other actinides, and the rare earths. Alkali and alkaline earth metals have received little attention due to their low toxicity as well as difficulty to accumulate by biosorption [20]. Biosorption methods have also been studied and applied for other pollutants, such as removal of dyes and nitrates [9, 12, 23, 86, 93].

2.2.1 Mechanisms of biosorption

Biosorption of a metal may proceed by physisorption, chemisorption, or a combination of both. Physisorption, also called physical adsorption, includes the adsorption mechanism as well as adsorption of precipitates [20, 28, 91].

Chemisorption may occur on certain functional groups present on the biosorbent, such as amine and acetamido groups in chitosan and chitin, hydroxyl groups in polysacchardies, and amino, amido, sulfhydryl and carboxyl groups in proteins [91]. Such functional groups may be considered as “active” or “binding” sites. Chemisorption occurs via interaction with functional groups of the sorbent via ion-exchange, chelation, or formation of neutral complexes.

The mechanism of chemisorption depends strongly on experimental conditions, such as metal concentration and pH [28]. For many sorbents, accessibility to the active sites is a key parameter which can influence metal sorption. Accessibility to active sites is partially determined by the specific surface area of sorbent, and can further be limited by crystallinity, steric hindrances, and by hydration of the sorbent [22, 56, 64].

2.2.2 Interaction mechanisms of chemisorption on chitosan

The majority of the published literature on chitosan sorption focuses on the evaluation of sorption performance and not on evaluation or determination of the chemical mechanism of metal binding with chitosan. Even so, various methods have been used by different authors to confirm the complex between chitosan and different metals, including differential scanning calorimetry, infrared spectroscopy, nuclear magnetic resonance, circular dichromism, thermal gravimetric analysis, potentiometry and spectrophotmetry [74, 89]. There are two types of chitosan complexes defined by the mechanism of their formation: coordination complexes and ion associates.

It is widely accepted that the main mechanism of sorption occurs at the amine groups (-NH_2) of chitosan, although hydroxyl groups may also participate [21]. When protonated in acidic solution, the amine group becomes a site for electrostatic interaction with anionic metals or dyes [22, 23, 25]. The free amine group has long been recognized as capable of forming dative bonds with transition metals [54]. The sorption mechanisms in a given case will depend on the solution composition, concentration, presence of co-ions or ligands, pH, and metal speciation [21]. The metal ion may also form complexes with other ligands in solution, thus changing its speciation. A cationic metal may form an anionic species with the ligand. For example, in strong nitrate media UO_2^{2+} forms the anionic species $[UO_2(NO_3)_4]^{2-}$. The speciation of the metal determines the mechanism of complexation with chitosan [25, 55].

2.2.2.1 Coordination complexes

Many studies have focused on the interaction of chitosan with Cu(II), leading to two common interpretations of the mechanism: the bridge model and the pendant model. In the bridge model, the metal ion is bound by inter- or intra-molecular complexation on multiple amine groups. In the pendant model the metal ion hangs like a pendant from only one amine group, with charge balanced by hydroxyl groups or water [21].

Park et al. studied the chitosan-Cu(II) interaction spectrophotometrically and de-

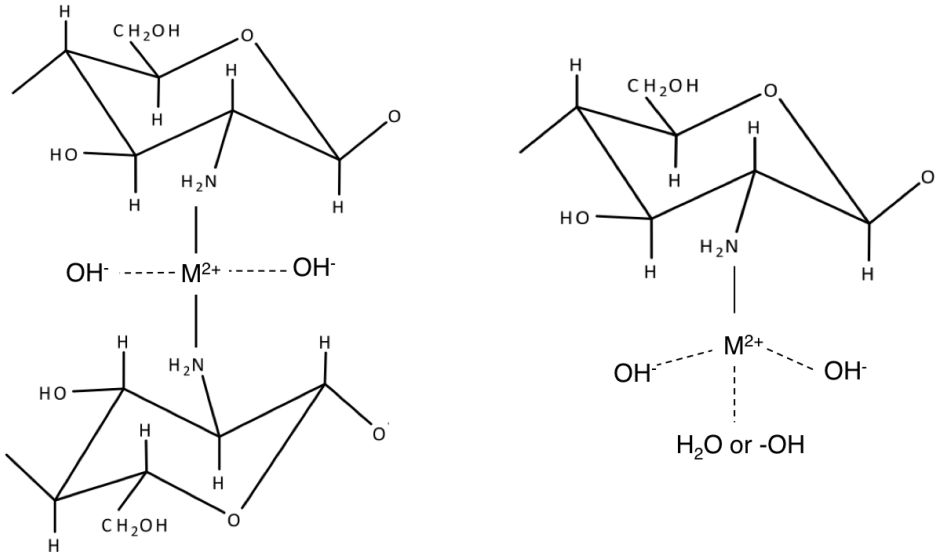

Figure 2.2: The bridge (left) and pendant (right) models of chitosan-metal complexation. *Adapted from [73].*

termined that concentration-dependent intra- and inter-molecular binding occurred. These authors also report that the addition of chloride salts appear to promote intermolecular binding, likely due to decreased electrostatic repulsion between chitosan chains due to the presence of Cl^- [61]. The authors also suggest that the disagreement between some chitosan-metal stability constants could be due to the formation of insoluble metal hydroxides which were interpreted as "chelated" to chitosan, when in fact, they were just physisorbed. The authors claim that such precipitation of metals on chitosan explains the sensitivity of chitosan-metal sorption rate and capacity to stirring, temperature and crystallinity [61].

Dambies et al. used x-ray photoelectron spectroscopy to investigate the chitosan-copper complex. These authors found that copper sorption resulted in a charge transfer from nitrogen to copper, supporting the hypothesis that sorption occurs on the amine groups. They also concluded that, based on the results of experiments at two pHs, the sorbed copper species were likely copper hydroxide, suggesting a combined sorption/precipitation mechanism [15]. The importance and role of metal hydrolysis on biomass sorption has also been addressed by Gadd and White, for the case of

actinides, which are readily hydrolyzed, and by Varma for the case of silver [4, 20, 89].

Piron and Domard found results of FTIR and UV-vis studies of chitosan-uranyl complexation to be in agreement with the pendant model for sorption of uranyl to chitosan, with the charge of the uranyl cation balanced by hydroxyl groups (assumed due to the absence of nitrate in the complex) [67].

Coordination of metals with the aminogroup of chitosan has also been reported for alkaline earth metals in alkalinic carbonate media. Piron and Domard studied ternary complexes of alkaline earth metals, strontium and barium, with chitosan [66]. The authors observed sorption at alkaline pH in carbonate solutions, and acknowledge possible dehydrating and other effects of carbonate anions on chitosan.The proposed mechanism is complexation of $Sr^{2+}CO_3^{2-}$ with chitosan. By varying the ionic strength of the solution, they found evidence that the sorption mechanism was not electrostatic, nor due to precipitation of the metals [66].

Studies of the complexation of the monomer unit, D-glucosamine, have been performed, but it is generally accepted that the polymer results in more efficient sorption, which has been used as evidence for the role of adjacent amine or hydroxyl groups in the sorption mechanism [21, 48, 61]. Recent work by Levitskaia et al. focused on the complexation of D-glucosamine and neodymium. By photospectrometric titration these authors found the formation constants and log β of Nd-D-glucosamine complexes and determined that the complexation occurs via a ligand-controlled hydrolysis mechanism. This is of note as it confirms the complex formation of the chitosan monomer with a model trivalent lanthanide, as well as opens the door to use of chitosan and chitosan derivatives for therapeutic lanthanide agents [48].

2.2.2.2 Ion associates

When the amine groups of chitosan are protonated, complexation can occur via the ion association mechanism when anionic species of the metal are attracted to positively charged (protonated) amine groups. The protonation of the amine groups is determined by the pKa, which in turn depends on the DDA of the chitosan [84]. This can be seen by observing the relationship between the dissociation degree, α, on DDA

and pKa [84]:

$$\alpha = \alpha' + \frac{[H^+]}{[NH_2]} \tag{2.1}$$

$$pK_a = pH + \log\left(\frac{1-\alpha}{\alpha}\right) \tag{2.2}$$

where α' is the experimental neutralization degree and $[NH_2]$ is the concentration of amine groups, which varies with DDA. The dissociation of chitosan is described by

$$\text{Chitosan}-NH_2 + H_3O^+ \rightleftharpoons \text{Chitosan}-NH_3^+ + H_2O \tag{2.3}$$

The dissociation constant, K_a, of chitosan is thus

$$K_a = \frac{[-NH_2][H_3O^+]}{[-NH_3^+]} \tag{2.4}$$

When pH = pKa, half of the amine groups will be protonated. The pKa of chitosan ranges from 6.3 to 7.2. Thus, at acidic pH, the majority of amine groups will be protonated and positively charged, and thus more likely to form ion associates with anions than to form complexes via an exchange of protons with cations. Ion associate mechanisms in chitosan sorption can be investigated by varying the ionic strength; such interactions will be sensitive to a change in ionic strength, as those ions will compete for binding sites [27, 90].

Publications on ion exchange mechanisms are limited to anionic species, including metal anions as well as anionic dyes. Guibal et al. investigated the sorption of vanadate and molybdate species onto chitosan, with maximal sorption at a pH (pH=3) corresponding to a predominance of protonated amine groups as well as the existence of polynuclear anionic hydrolyzed species [22]. Guibal et al. found that dissolved chitosan was superior to solid chitosan for sorption of anionic dyes. This was attributed to the increased number of available amine groups, which are made available by the breaking of inter- and intra-chain hydrogen bonding involving the amine groups when the polymer is dissolved [23]. A similar increase in sorption for anionic dyes was ob-

served by Trung et al. using decrystallized chitosan [86].

2.3 Evaluation of sorption: isotherms and kinetics

The evaluation of a biosorbent for sorption of a given metal includes determining its capacity for the metal via isotherm modeling and determining its kinetics. Isotherm modeling can be accomplished using the classical Langmuir and Freundlich isotherms. Biosorption kinetics have usually been found to be described by the pseudo- first and second order rate equations [28].

2.3.1 Kinetics of biosorption

A study of the kinetics of a biosorption system is necessary to determine the rate-limiting step(s) of sorption and the kinetic parameters. These parameters are necessary for implementing a large-scale sorption system, to determine optimal contact time and maximum sorbent capacity [51]. Additionally, knowledge of the rate-limiting step(s) of sorption, as well as the kinetic model, can provide insight to the nature of the sorption mechanism [28]. For example, The sorption process is considered to be composed of four steps: (1) transport of the solute from the bulk solution to the sorbent boundary film (bulk diffusion); (2) diffusion of the solute from the boundary film to the sorbent surface (film diffusion); (3) diffusion of the solute from the sorbent site to intraparticle spaces/ pores of the sorbent (intraparticle diffusion); (4) sorption (or desorption) of the solute at active sites on the surface and pores of the sorbent [24, 28, 65, 68]. The entire sorption process is thus affected by changes to any step, and these steps can be affected by many experimental conditions, including particle size, agitation rate and pH, among others [19, 28]. It is generally accepted that vigorous agitation is sufficient to eliminate steps (1) or (2) from being rate-limiting [24, 28, 68]. Thus, many kinetic models that have been developed for biosorption systems consider step 3 or 4 to be rate limiting.

Various kinetic models have been developed in order to determine or predict which steps are rate limiting. It is possible for there to be more than one rate limiting

step, and also possible for the rate limiting step to change over the course of the contact time. Many commonly used kinetic models, however, assume only one rate limiting step, which can make it difficult to model the data over the entire sorption time with only one mathematical model. Many commonly-used models assume that step (4) is rate limiting, and refer to this step as the *surface reaction*, which may be either a chemical reaction occurring on the surface or a physisorption interaction [68]. The most common of these models, as applied to biosorption systems, are the pseudo-first (Lagregen) and pseudo-second order kinetic equations. Models that consider step 3, the diffusion step, are referred to as the diffusion models; the most common of these is the intraparticle diffusion model (Weber-Morris model) [45]. Many other kinetic models exist, but were not applied in this work. It should be noted that while some of the kinetic models have theoretical bases, others do not.

2.3.1.1 Pseudo-first order model

What is now known as the pseudo-first order kinetic model was introduced by Lagergren to empirically describe adsorption of acids onto charcoal, and it is considered to be one of the first equations describing sorption rates for liquids onto solids [68]. It is described by the differential equation

$$\frac{dq(t)}{dt} = k_1(q_e - q(t)) \tag{2.5}$$

where $q(t)$ is the sorption capacity (mg/g) at time t, and q_e is the sorption capacity at equilibrium. When equation 2.5 is solved using the boundary conditions $q(t) = 0$ when $t = 0$ and $q(t) = q_e$ at $t = e$ we obtain:

$$q(t) = q_e(1 - e^{-k_1 t}) \tag{2.6}$$

where $q(t)$ and q_e are sorption capacity (mg/g) at times t and equilibrium, as before, and k_1 is the pseudo-first order rate constant, with units of inverse time. This can be

linearized to the following equation:

$$\ln(q_e - q(t)) = \ln(q_e) - k_1 t \tag{2.7}$$

The parameter k_1 determines how fast the system reaches equilibrium; increasing k_1 results in equilibrium being attained more quickly. The linearized form, equation 2.7, is usually used to fit data. However, this method requires knowledge of the equilibrium sorption capacity, q_e, which is not always known for the conditions of the kinetic experiment. Problems obviously arise when $q(t) > q_e$, which may arise if q_e is not known well.

2.3.1.2 Pseudo-second order model

The pseudo-second order kinetic model is described by the differential equation

$$\frac{dq(t)}{dt} = k_2(q_e - q(t))^2 \tag{2.8}$$

where $q(t)$ is the sorption capacity (mg/g) at time t, and q_e is the sorption capacity at equilibirum. When equation 2.8 is solved using the boundary conditions $q(t) = 0$ when $t = 0$ and $q(t) = q_e$ at $t = e$ we obtain:

$$q(t) = \frac{k_2 q_e^2 t}{1 + k_2 q_e t} \tag{2.9}$$

where $q(t)$ and q_e are as before, and k_2 is the pseudo-second order rate constant ($\text{mg}\cdot\text{g}^{-1} \cdot t^{-1}$). Equation 2.9 can be linearized to the following equation:

$$\frac{t}{q_t} = \frac{1}{k q_e^2} + \frac{t}{q_e} \tag{2.10}$$

Equation 2.10 is not a unique linearization of Equation 2.9, as there are four commonly used linearized forms of the pseudo-second order equation. Equation 2.10 is the most commonly used linear form, however, and it generally results in good fits of many biosorption processes [28]. An advantage of this model is that it can be used to deter-

mine the equilibrium sorption capacity, q_e, and is less sensitive to experimental error than the other models [68]. This may contribute to the observed good fits of this model to diverse data sets.

2.3.1.3 Elovich model

The Elovich equation was introduced in 1934 by Roginsky and Zeldovich to describe adsorption kinetics of carbon monoxide on manganese dioxide [68]. It is given by

$$q(t) = \frac{1}{\beta} \ln(1 + \alpha\beta t) \tag{2.11}$$

where α (mg $g^{-1}t^{-1}$) and β (g/mg) are the Elovich constants. It should be noted that as $t \to \infty$ the model results in non-physical behavior; the model is therefore more appropriate to describe the initial stages of sorption. Many of the theoretical interpretations of the Elovich equation assume heterogeneity of the sorbent surface [68]. It has also been shown that the Elovich and psuedo-second order models behave almost identically when the fraction surface coverage of adsorbent is less than 0.7 [68]. A generalization of the Elovich equation was derived by Rudinski and Plazinski using statistical rate theory [68].

2.3.1.4 Intraparticle diffusion model

When intraparticle diffusion is the rate limiting step, the sorption capacity ($q(t)$) will vary linearly with the square root of contact time:

$$q(t) = k_d\sqrt{t} + C \tag{2.12}$$

where k_d is the intraparticle diffusion rate constant (mg $g^{-1}t^{-1/2}$) and C (mg/g) is a constant related to the thickness of the boundary layer around sorbent particles [28]. It is possible for multi-linearity to exist in the model, corresponding to diffusion in increasingly smaller or deeper pores of the sorbent [51].

2.3.2 Sorption isotherms

Sorption isotherms describe the retention of a sorbate on a sorbent under varying sorbate concentrations. Given a concentration of sorbate, C, and the concentration of sorbate retained on the sorbent, q, then a function f such that $q = f(C)$ is called the *sorption isotherm* [50]. To determine a sorption isotherm empirically requires collecting data of the sorption system at equilibrium with varying sorbate concentrations under otherwise identical conditions; *isotherm* thus implies not only a constant temperature throughout the process, but also constant pH, ionic strength, and so forth [50].

Brunnauer et al. classified five shapes of isotherm for adsorption by van der Waals forces. Giles, in a later classification, proposed four main shapes, shown in Figure 2.3 [50]. The "C" type is linear, wherein the distribution coefficient is constant for all sorbate concentrations. The sigmoidal "S" type arises from the result of two opposite sorption mechanisms. One example of this is in the case of a ligand in aqueous solution with a metal ion; at low concentrations, the ligand and sorbent compete for the metal, where at high concentrations of metal, the ligand will be saturated with metal and excess metal can be sorbed. The "L" type isotherm results when the distribution coefficient decreases with increasing sorbate concentration, which may be due to the sorbent tending toward saturation. Examples of "L" type isotherms are the Freundlich, Langmuir, Temkin, Redlich-Peterson and Toth isotherms. The Freundlich and Langmuir are the most applied and perhaps best studied of these, and are discussed here. The "H" type isotherm is a special case of the concave "L" type isotherm; the "H" type is characterized by a very steep initial slope.

2.3.2.1 Freundlich isotherm

The Freundlich isotherm was one of the earliest empirical models proposed to describe sorption systems [50]. It is given by

$$q_e = KC^n \tag{2.13}$$

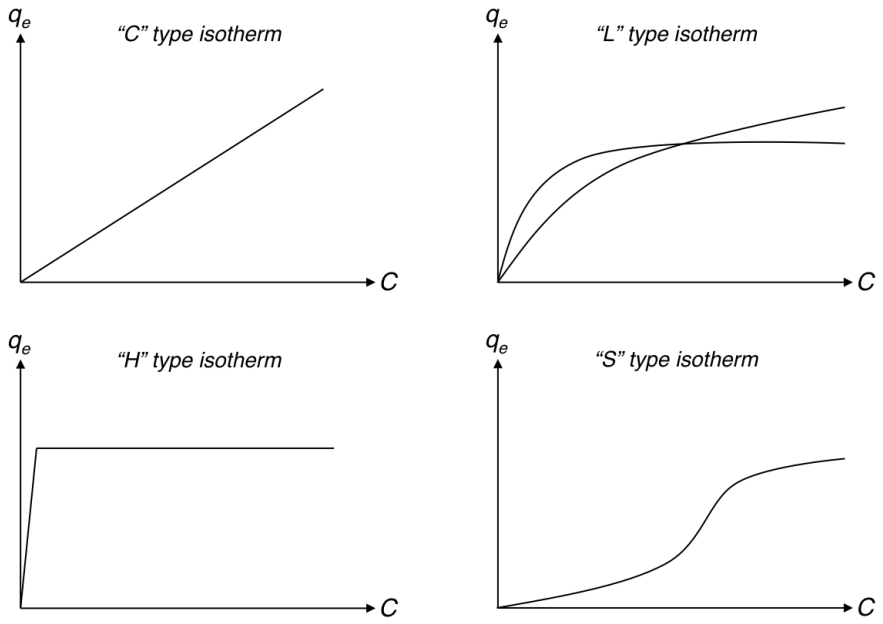

Figure 2.3: The four isotherm shapes, as classified by Giles. *Adapted from [50].*

where q_e is the equilibrium sorption capacity, C_e is the equilibrium sorbate concentration and K and n are the model parameters, with the restriction $n < 1$. Mathematically, for all n and K, it can be seen that q_e does not reach a limit as $C_e \to \infty$, and so the isotherm does not reach a plateau. While this isotherm was originally derived empirically, a theoretical derivation is presented by Skopp [83].

2.3.2.2 Langmuir isotherm

The Langmuir isotherm was proposed by Irving Langmuir in 1918. In fact, six different cases were considered by Langmuir, but it is the first case, "simple adsorption", which has been the most widely applied; the other models can be viewed as generalizations to cases such as multi-site adsorption [46]. The simple case is based on the assumptions that all adsorption sites are identical; each site can only adsorb one molecule; and all sites are energetically and sterically independence of the adsorbate. Starting with the kinetic gas theory, Langmuir derives the relationship which can be

written as

$$q_e = \frac{q_m K C_e}{1 + K C_e} \tag{2.14}$$

were q_e (mg/g) and C_e (mg/L) are the sorption capacity and concentration and equilibrium, respectively. The equation parameters are q_m and K; q_m (mg/g) is the maximum adsorption capacity and K is the Langmuir affinity constant (L/mg), which describes the strength of interaction between the sorbate and sorbent. It can be seen that as $C_e \rightarrow \infty$, q_e approaches the limit of the value of the parameter q_m, resulting in a plateau. It should be noted that the assumptions of the Langmuir isotherm are seldom met in the case of biosorption systems. However, it has been found that kinetics of biosorption systems have been reasonably well modeled by the simple Langmuir isotherm.

3 Materials and Methods

3.1 Materials

3.1.1 Chitosan

Chitosan was purchased from Sigma-Aldrich (St. Louis, MO) or used as received from the Oregon Biomedical Engineering Institute (OBEI, Portland, OR). Five types of chitosan were received from OBEI, which were assigned codes A–E. Types A and C were in the physical form of flakes/fibers and types B, D and E were in a powder form.

3.1.2 Radiotracer Solutions

Uranyl nitrate hexahydrate (Fisher) was dissolved in 0.1 M $HClO_4$ to produce a 0.2 M UO_2^{2+} stock solution. The stock solution was used to make subsequent dilutions for use in experiments.

^{60}Co stock solution was prepared from an in-house stock solution produced by neutron activation in the Oregon State TRIGA reactor facility (OSTR). The ^{60}Co stock received was converted to the nitrate form, $Co(NO_3)_2$, by repeated evaporation to dryness in an excess of concentrated nitric acid. Stock solution was made by dissolving the resulting $Co(NO_3)_2$ in 1 M HNO_3. The ^{60}Co concentration was determined by radiometric analysis using an energy and efficiency calibrated high purity germanium detector. The chemical concentration of cobalt in the stock was determined by UV-visible spectroscopy of the cobalt absorption band at 505 nm and found to be 0.03 M. A solution of non-radioactive cobalt was prepared by dissolving $Co(NO_3)_2 \cdot 6\,H_2O$ in 1 M HNO_3 with cobalt concentration 0.2 M.

^{152,154}Eu stock was received in the nitrate form, $Eu(NO_3)_3$, dissolved in 1 M nitric acid, with europium concentration 2.5 mM. This stock had previously been produced by neutron activation in the OSTR. A stock solution of non-radioactive europium was prepared by dissolving Eu_2O_3 in 1 M HNO_3 to produce a 0.1 M europium concentration.

All other reagents were of analytical grade and were used as received.

3.2 Sorption experiments

Working solutions of each cation were prepared from dilutions of the radiotracer stock solutions in DI water. Chemical concentration of the solutions was adjusted by addition of the non-radioactive solutions (except for uranium). The pH of each solution was measured using an Orion 410A or Thermo Orion 3-star pH meter and was adjusted as necessary by addition of strong NaOH or HNO_3 (for uranium, NaOH or $HClO_4$).

To determine sorption isotherms and kinetics, a given volume of metal solution (ranging from 1 mL to 10 mL) with a known concentration (10 to 2,000 mg/L) was added to plastic screw-top vials (2 mL, 4 mL or 15 mL) containing a given mass of sorbent at room temperature (20°C $\pm$ 2°C) or at elevated temperature (37°C $\pm$ 1°C). After addition of the metal solution, each vial was briefly vortexed and then agitated for the desired contact time (ranging from 10 minutes to 168 hours). Agitation was performed on either a Labquake end-over-end shaker or a Eppendorf Thermomixer R mixer incubator. At the end of contact time, the vials were centrifuged and an aliquot of the supernatant was taken to determine the concentration of metal remaining in solution. For kinetic experiments, subsequent aliquots were taken from the same vial at differing contact times. In this case, samples were centrifuged, an aliquot taken, re-vortexted and returned to the agitator until the next sampling time. Control experiments, containing no chitosan sorbent, were performed to verify the absence metal sorption on the vial walls or precipitation of metal due to hydrolysis or other mechanism. The pH of solutions was measured after the final aliquots were taken using an Orion 410A pH meter.

3.3 Analysis of solutions

Determination of cobalt and europium concentration in solutions was done by radiometric analysis. A Packard Cobra II sodium iodide (NaI) scintillation detector was used for all radiometric analyses. The counting window used for ^{60}Co spanned 1025 to 1425 keV, including the ^{60}Co gamma emissions at 1173 and 1332 keV. The counting window used for ^{152,154}Eu spanned 300 to 390 keV, which includes the 344 keV gamma resulting from the ^{152}Eu beta decay. The choice of window was constrained by the resolution of the detector. The counting time was adjusted to result in counting error of less than 2%. Each experimental sample was compared to a reference sample of the initial metal solution, eliminating the need to include the efficiency of the detector in calculations. The concentration of residual metal in solution was calculated using the activity concentrations of the sample and reference. The gamma peak at 661 keV was used for determination of ^{60}Co activity and the peak at

Uranium concentration was determined by the Arsenazo(III) method using an Ocean Optics QE65000 or Olis RSM-1000 UV-vis spectrometer. Spectra were recorded in the UV-visible region from 450 to 700 nm using 1 cm cuvettes. The absorbance of the Arsenazo(III)-uranyl complex band at 651 nm was used for analysis. Beer's law was found to be obeyed up to a uranium concentration of 3.5×10^{-5} M. Below this concentration absorbance of the complex is proportional to uranium concentration.

3.4 Fourier Transform Infrared Spectroscopy

FTIR analysis was conducted on a Nicolet 6700 spectrometer equipped with diamond hastloy attenuated total reflection (ATR) plate. Powder samples were prepared for analysis by drying, either in dessicator, oven, or open air. The IR spectrum was recorded in the wavenumber range from 4000 to 700 cm^{-1} using 32 scans with resolution of 2 or 4 cm^{-1}.

3.5 Evaluation of experimental results

The uptake (%), distribution ratio (K_D), and adsorption capacity (q) of the chitosan sorbents were determined by a mass balance equation. The adsorption capacity, q_t (mg/g), was calculated at time t as

$$q_t = (C_0 - C_t)\,\frac{V}{m} \tag{3.1}$$

where C_0 is the initial metal concentration in solution (mg/L), C_t is the metal concentration in solution at time t, and m and V are the mass of sorbent (mg) and volume of aqueous metal solution (mL), respectively. The distribution ratio, K_d (L/g), was found as

$$K_d = \left(\frac{C_0 - C_f}{C_f}\right)\frac{V}{m} \tag{3.2}$$

where C_0 and C_f are the initial and final metal concentrations in solution (mg/L), respectively, V is the volume of aqueous metal solution (mL) and m is the mass of sorbent (mg). The uptake, expressed as a percentage, is found by

$$\mathrm{U}(\%) = \frac{C_0 - C_f}{C_0} \tag{3.3}$$

where C_0 and C_f are defined as above. The residual concentration of metal remaining in solution, C_f, was calculated by

$$C_f = \frac{C_0}{A_0}A_f \tag{3.4}$$

where C_0 is the initial concentration, and A_0 and A_f are the initial and final measured activity concentrations (Bq/mL), respectively. In the case of uranium, A_0 and A_f are the initial and final absorbances of the Arsenazo(III)-uranyl complex measured at 651 nm in 1 cm cuvettes, and thus the ratio of initial and final absorbances is equal to the ratio of the initial and final concentrations.

3.6 Modeling of adsorption kinetics and isotherms

Modeling of adsorption kinetics and isotherms was done using R, version 2.13.1 (R Foundation for Statistical Computing) [**o**]r Excel (Mircrosoft). R was used for linear and nonlinear least squares regressions; Excel was used only for ordinary least squares regression. The nonlinear least squares method in R implements a Gauss-Newton algorithm.

3.7 Goodness-of-fit

The goodness-of-fit of isotherm and kinetic models was evaluated using the residual root mean square error (RMSE), sum of squared errors (SSE), and correlation coefficient (R^2). The RMSE is found as

$$\text{RMSE} = \left(\frac{\sum_{i=1}^{m} (n_i - \hat{n}_i)^2}{m - p} \right)^{1/2} \tag{3.5}$$

where $\hat{n}_i$ is the model predicted value for observation n_i, m is the number of observations and p is the number of adjustable parameters. The RMSE, as calculated above, is the estimated standard deviation of the errors. It should be of similar size to estimates of the measurement errors. Larger values of RMSE indicate that another source of error is present, and may be indicative of a lack of fit of the model [43].

The SSE is found as

$$\text{SSE} = \sum_{i=1}^{m} \frac{(n_i - \hat{n}_i)^2}{n_i^2} \tag{3.6}$$

where $\hat{n}_i$ is the model predicted value for observation n_i and m is the number of observations. The SSE will be minimized when the model parameter estimates ($\hat{n}_i$) approach the observed values (n_i), thus, a smaller SSE is indicative of a better fitting model [28].

The correlation coefficient is calculated as

$$R^2 = \frac{\sum_{i=1}^{m} (n_i - \bar{n}_i)^2 - \sum_{i=1}^{m} (n_i - \hat{n}_i)^2}{\sum_{i=1}^{m} (n_i - \bar{n}_i)^2} \tag{3.7}$$

with variables as defined above. The correlation coefficient captures the the fraction of variance (about the mean) explained by the model [43].

4 Results and Discussion

4.1 Sorption of radionuclides by chitosan

The sorption of cations by chitosan was found to be dependent on pH, contact time, and initial metal concentration. These are discussed in the sections below.

4.1.1 Effect of pH

Solution pH affects both the speciation of the metal and the protonation of chitosan amine groups. Both of these factors influence the adsorption process, and so an examination of the effect of pH on adsorption efficiency is necessary in order to optimize an adsorption system.

Chitosan has an intrinsic pK_0 of around 6.5 and dissolves in most organic and mineral acids (with the exception of sulfuric acid) [84]. In acidic solutions, the amine group (-NH_2) of chitosan becomes protonated. The protonated amine has been determined to be a site for anion sorption on chitosan, as it allows for an ion association interaction to take place [22, 42]. However, a strong protonation of the amine groups results in a decrease of sites available for complexation with cations via other mechanisms, such as the formation of coordination complexes.

The speciation of metal cations in solution is dependent on the pH of the solution, the concentration of the cation, and the concentration of other ions in solution. Many cations undergo hydrolysis, resulting in the formation of metal hydroxides. The hydrolysis of a metal cation M^{j+} can be written as:

$$M^{j+} + kH_2O \rightleftharpoons M(OH)_k^{(j-k)+} + kH^+ \tag{4.1}$$

When j = k, the species has no charge, and may precipitate from solution. The hydrolyzed species typically have a lower solubility than non-hydrolyzed species, which can also lead to their precipitation from solution. The formation of polynuclear species, such as $M_i(OH)_k^{(ij-k)+}$ is also possible, which may result in steric hindrances toward

complexation with an active site which are not present with mononuclear species. Precipitation of the metal interferes with determination of the amount of metal sorbed by chitosan, as the mass-balance equation used assumes that any metal not remaining in solution is sorbed by the sorbent. Precipitated species are removed from solution but are not necessarily sorbed by chitosan, and thus the calculation of metal sorbed to chitosan may be erroneous.

The effects of initial solution pH on sorption were investigated for cobalt and europium. The pH dependence of uranium was not studied, due to its strong tendency to from hydrolyzed species at pH above 4.5 under the experimental conditions, and the dissolution of the sorbent at lower pH.

Figures 4.1 and 4.2 show the effects of initial solution pH on the chitosan sorption (uptake) of Eu(III) and Co(II), respectively. It can be seen that in this pH range, europium adsorption onto chitosan is not strongly dependent on pH and varies similarly for both types of chitosan used. The pH range studied was constrained by the solubility of the sorbent at lower pH and by precipitation of the metal at higher pH. At the highest initial pH tested, pH = 8, Eu precipitated from solution in the absence of any sorbent, as verified by the sorbent-free control sample.

The lower metal uptake at low pH may be due to a combination of factors, including (1) the competition between protons and metal cations for binding sites; (2) partial dissolution of the sorbent and (3) the speciation of the metal. The speciation of metal is highly dependent on pH and the presence of other ions in solution. As pH increases, the dominant species in solution will change from un-hydrolyzed species Eu^{3+} or Co^{2+} to hydrolyzed species such as $Eu(OH)_2^+$ or $Co(OH)^+$. A speciation model[1] relevant to the conditions of the europium experiment is shown in Figure 4.3, which shows the distribution of Eu species, expressed as the logarithm of Eu concentration, as pH changes. At acidic pH (below pH 6.5), the dominant species is free Eu^{3+}, whereas at higher pH (above 6.5), the dominant species is the crystalline hydroxide complex, $Eu(OH)_3(c)$. At near-neutral pH under these conditions, five europium species coexist:

[1]Speciation model was created using the Hydra and Medusa software package [69].

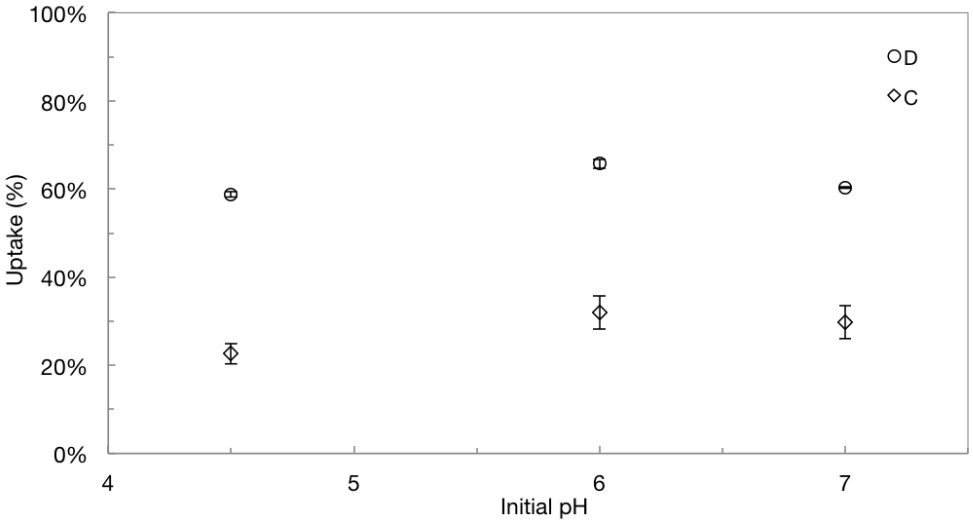

Figure 4.1: Effect of pH on sorption of Eu(III) by two types of chitosan, with 5 g/L chitosan and 100 mg/L Eu(III). Error estimates from duplicate samples; note that error bars for chitosan D are within the marker symbol.

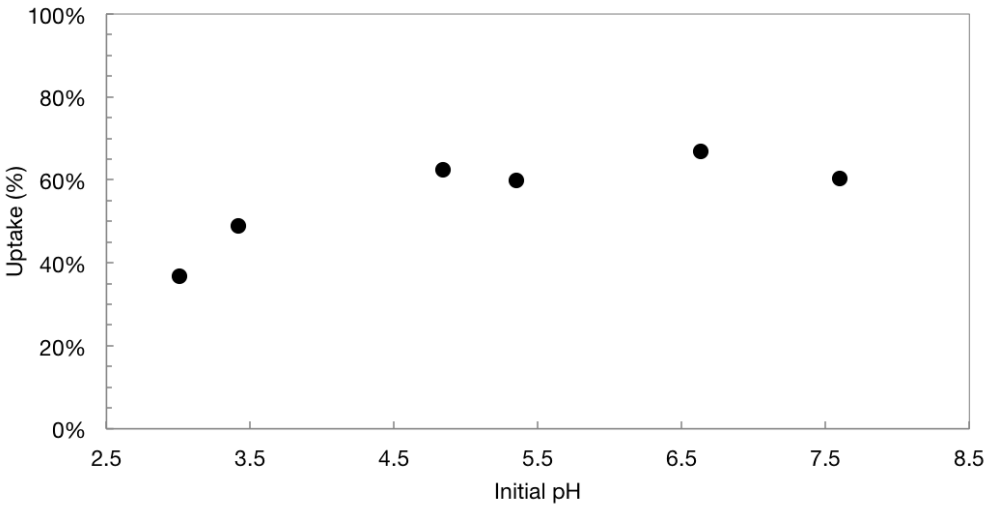

Figure 4.2: Effect of pH on sorption of Co(II) by chitosan D, with 5 g/L chitosan and 50 mg/L Co(II).

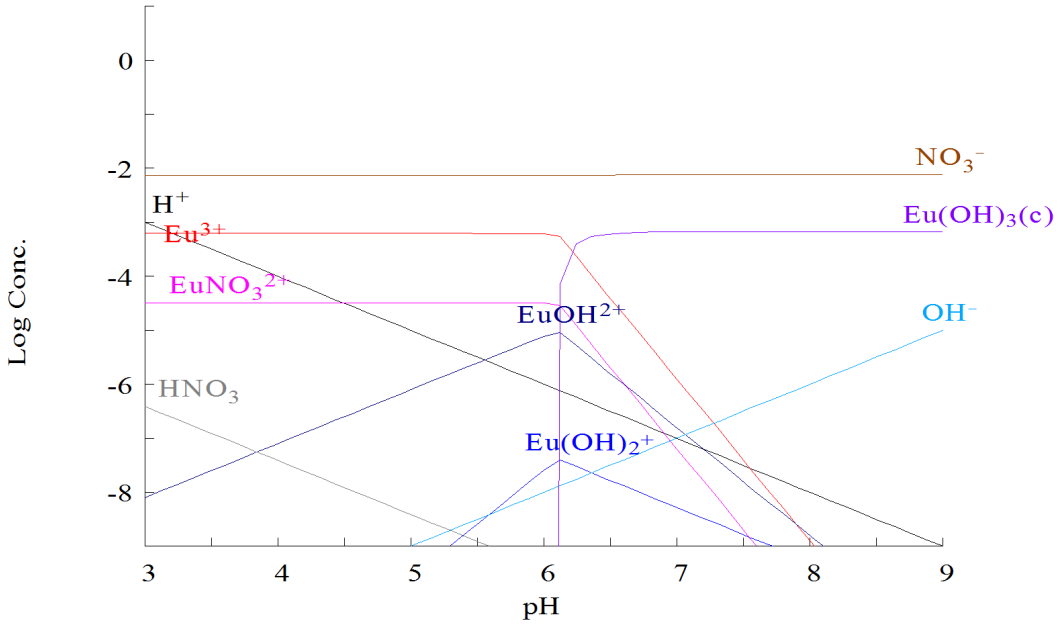

Figure 4.3: Speciation of 100 mg/L Eu(III) in aqueous solution, with $[NO_3^-]$ = 7.5 mM, as a function of pH. Crystalline (precipitated) species is denoted by the symbol (c).

free Eu^{3+}, the mononitrate species $EuNO_3^{2+}$, and hydroxide species $Eu(OH)^{2+}$, $Eu(OH)_2^+$ and the crystalline $Eu(OH)_3$.

The formation of chitosan-europium and chitosan-cobalt complexes may depend on the speciation of the europium or cobalt. If chitosan-metal complexes form more favorably with hydroxide species than with nitrate species or free Eu^{3+} or Co^{2+}, we may expect a corresponding increase in sorption when hydroxide species become relatively more abundant, around pH 6 in these conditions.

The final pH of the chitosan-europium solution was measured at the end of the contact time (except for initial pH = 8). As shown in Table 4.1, the pH of the solutions ranged from 6.2 to 6.8 after contact with the chitosan sorbent. The pH of control samples (containing no sorbent) remained within 0.5 pH units of initial pH; hence the change in pH of the solutions was due to the presence of chitosan.

It is possible that the pH of the solution during the majority of the sorbent-solution contact time influences the sorption process, and thus final uptake, more than

Table 4.1: Measured pH of europium solutions after 1 hour contact with chitosan.

Initial pH	Final pH	
	C	D
4.5	6.52	6.55
5	6.53	6.71
6	6.25	6.43
7	6.60	6.72

the initial pH does. Such a phenomena could explain the observed weak dependence of sorption uptake on pH, as the final pH of each europium solution was observed to vary by less than 0.5 units when the initial range was 2.5 pH units. Maintaining a constant pH throughout the entire contact time may provide more insight to the role of pH on sorption. If a different pH dependence is found when the solution pH is kept constant throughout the contact time it may be concluded that the weak dependence on pH observed here is due to the small range of final pH. While it would be desirable to maintain constant pH by use of a buffer, it was not experimentally practical to do so here. The pH range investigated would require the use of several different buffers. To avoid interference of the buffer with the cation in solution, each buffer would ideally be non-complexing. Additionally, the interaction of each buffer with the sorbent itself would need to be determined and accounted for. For example, it has been shown that the acetate anion (present in acetate buffer) can be sorbed by the amine groups of chitosan [26, 80]. Acetate and MES buffers were used in the course of this experimental work and were found to interact and interfere with the chitosan sorbent. Thus, pH was not controlled by buffer, nor was it adjusted throughout the course of the sorption time. Non-complexing buffers were not available for each pH range of interest. Non-complexing buffers were desired for use, as some common buffers (phosphate, acetate) are known to form complexes with cations in solution. Such complexes may interfere with the chitosan sorption mechanisms in a manner that could not be accounted for [94].

To determine the cause of the increase in final pH of chitosan-metal solutions,

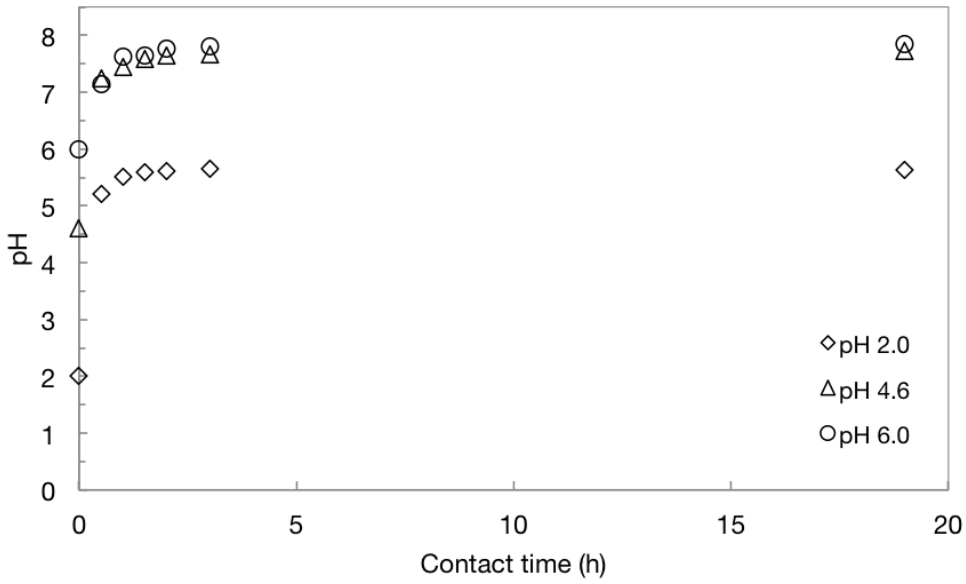

Figure 4.4: Change in pH of acidic solutions (initial pH = 2, 4.6 or 6) as a result of contact with chitosan D. Acid solutions without chitosan remained $\pm$ 0.1 pH unit of initial pH throughout experiment.

chitosan was contacted with acidic solutions in the absence of any metal cations. A definite increase in solution pH as a function of contact time was observed, as shown in Figure 4.4. The observed increase in solution pH can be attributed to the protonation of chitosan: as the amine groups become protonated (-NH_3^+), protons are removed from solution, resulting in an increase of solution pH. The pH of the solutions increased until equilibrium pH was reached after three hours, which provides an indication of the hydration kinetics of the polymer. We observe that even with an initial pH = 2, the final pH is increased to pH 5.5 due only to the chitosan. Mizera et al. also reported this effect, due to the buffering effect resulting from the amine group, with pK_a around 6.5 [53].

4.1.2 Effect of contact time

Experiments to determine the sorption uptake kinetics of uranium, europium, and cobalt by selected chitosans were performed using two types of chitosan: type C,

representative of the flake chitosan, and type D, representative of the powder chitosan. The effect of hydration and swelling of chitosan on uptake kinetics was investigated for europium, the effect of sorbent loading and agitation on uptake kinetics was investigated for uranyl, and the effect of temperature, sorbent loading, pH and metal concentration were investigated for cobalt.

For all three cations, it was observed that sorption onto the powder type D chitosan was greater than for the flake type C, as seen in Figures 4.5, 4.6, and 4.7, and that the majority of sorption occurs in the first 8 hours, with full equilibrium attained after a longer period (up to 72 hours or more). The differences in uptake between C and D can be attributed, in part, to the greater specific surface area of the powder chitosan. However, other differences between the two chitosans, such as their crystallinity and degree of acetylation, may also be responsible for the differing uptakes.

For Co(II) sorption on chitosan, the effect of temperature, pH, and metal concentration appear to have little effect on the time required to reach equilibrium sorption, but do affect the equilibrium sorption capacity. A discussion of these parameters is provided in section 4.2.

4.1.2.1 Effect of polymer hydration and pH

It is observed that equilibrium sorption was attained after approximately 24 hours for the powder chitosan, and after 72 hours for the flake chitosan, with an initial Eu(III) concentration of 50 mg/L, as shown in Figure 4.5. For both types of chitosan, initial uptake was greater for pre-wet chitosan than untreated (dry) chitosan. However, the magnitude of the increase in uptake was greater for the flake chitosan than powdered chitosan. The difference in uptake between pre-wet and untreated flake chitosan tended to decrease as the system approached equilibrium; after six hours, the uptake of pre-wet and untreated powder chitosan (D) were nearly identical. In contrast, the adsorption of the pre-wet flake (C) chitosan exceeded the untreated chitosan, even at 168 hours contact time.

The more rapid uptake in pre-wet chitosan indicates that ion mobility is increased in the pre-wet (hydrated) chitosan, or that hydration of the polymer by water

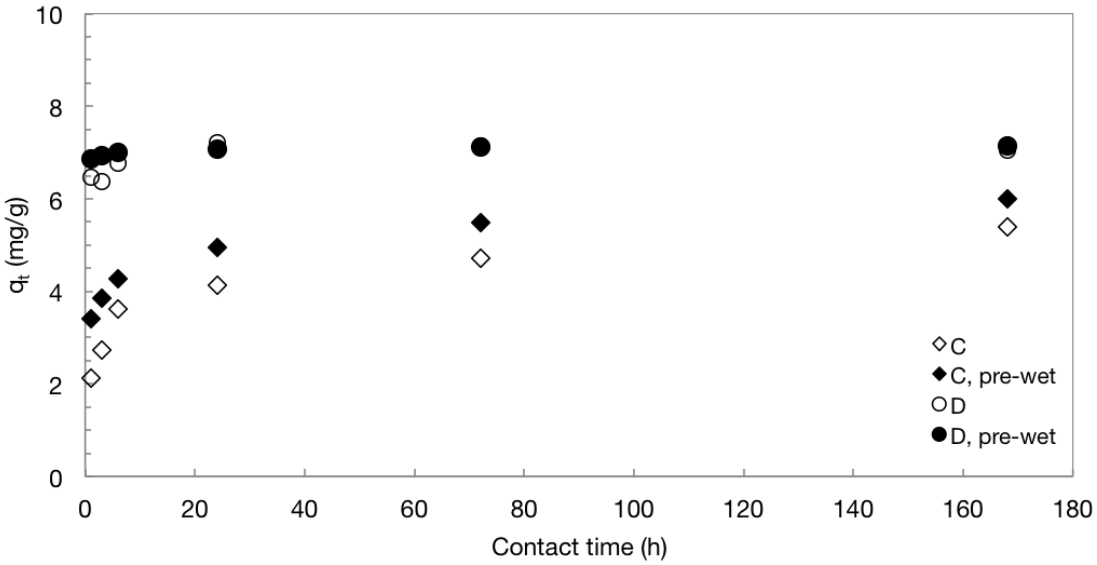

Figure 4.5: Effect of contact time and polymer hydration on sorption of Eu(III) by two types of chitosan (C, D). Conditions: 5 g/L chitosan, 50 mg/L Eu(III), initial pH = 5.

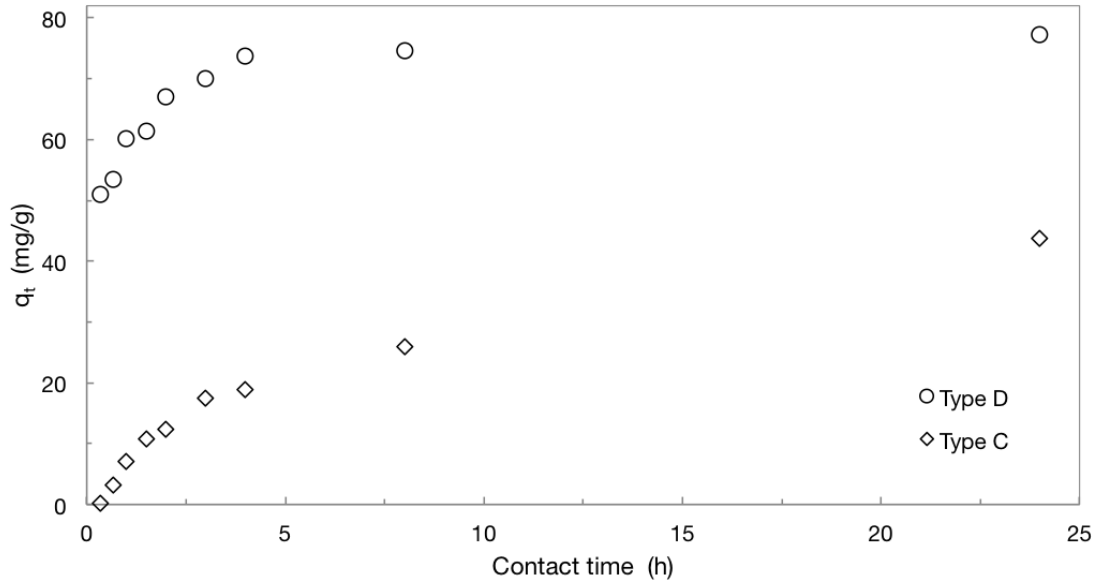

Figure 4.6: Effect of contact time and chitosan type on UO_2^{2+} sorption. Conditions: 2 g/L chitosan, 200 mg/L UO_2^{2+}, initial pH=4.6.

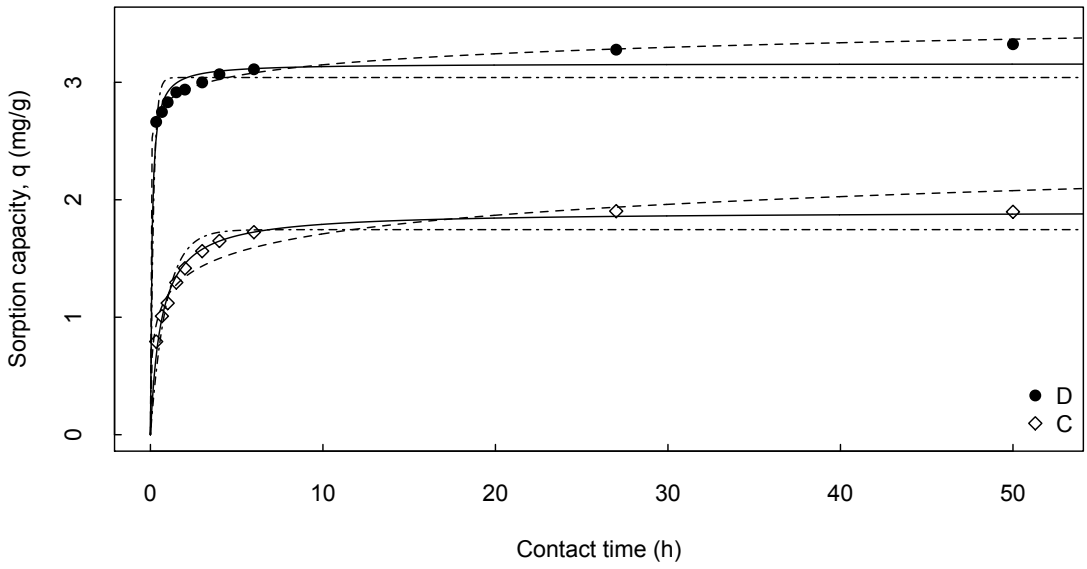

Figure 4.7: Effect of contact time and chitosan type on Co^{2+} sorption. Conditions: 10 g/L chitosan, 50 mg/L Co^{2+}, initial pH=6, T= 37 °C. Curves are fits of kinetic models, discussed in section 4.2.

increases the accessibility of binding sites on chitosan. It has been proposed that metal binding can only occur when chitosan is fully hydrated, allowing for the transport of cations to the active sites [64]. Due to the increased specific surface area of the powder type chitosan relative to the fiber type chitosan, it has a larger relative number of accessible binding sites prior to hydration of the polymer (i.e., the active sites on the surface, which are less affected by polymer hydration relative to interior binding sites). Thus, while hydration may increase the total number of accessible binding sites on the powder chitosan, the relative increase is not as pronounced as for the flake chitosan. If the initial increased uptake rate is due to the hydration or swelling of the polymer, it is expected that at equilibrium the uptake will be equivalent for both pre-wet and untreated chitosan, as the untreated chitosan will become hydrated during the long sorption time; the hydration time for pre-wet chitosan was 24 hours. Equivalent equilibrium uptake is observed for the pre-wet and untreated powder (D) chitosan, but not for the flake (C) chitosan.

The effect of polymer hydration on uptake was also investigated for UO_2^{2+} sorp-

Table 4.2: Uptake and sorption capacity for UO_2^{2+} sorption on pre-wet and dry chitosan. Conditions: 25 g/L chitosan, 200 mg/L UO_2^{2+}, pH = 4.6, T=20 °C.

Sorbent		q (mg/g)		Uptake (%)	
		dry	pre-wet	dry	pre-wet
Flake	A	5.6	7.4	73.0	93.9
	C	4.4	6.8	62.9	84.7
Powder	B	7.2	7.9	99.1	99.6
	D	7.8	7.8	99.4	99.2
	E	7.3	7.2	99.1	97.8

tion on chitosan. With a 1 hour soaking time, an increase in uptake and sorption capacity was observed, with a greater increase in uptake for flake-type chitosan (A, C) relative to the powder chitosan, as shown in Table 4.2. It should be noted that the uranyl uptake in the dry powder (types B, D, E) chitosan was already close to 100 percent, and thus any improvement resulting from pre-wetting was not observable.

In europium hydration studies the pH of the solutions were measured throughout the experiment and are shown in Table 4.3. After three hours contact time pH reached a plateau for all samples. For both types of chitosan, the pH of the pre-wet and untreated samples were very similar at each measurement. Increased uptake has been observed with increased final pH values in batch sorption experiments of chitosan with europium and other metals, suggesting a dependence of uptake on final pH. As there is only a small difference (< 0.15 units) in measured pH for pre-wet and untreated chitosans, the difference in uptake observed for the pre-wet and untreated fiber-type chitosan is not explained by a difference in pH alone. It is more likely that the difference in uptake, seen in Figure 4.5, is due to the increased accessibility of binding sites resulting from the hydration or swelling of the polymer.

4.1.2.2 Effect of agitation

Given the evidence that metal sorption occurs primarily on the highly accessible surface sites, the effect of agitation of the sorbent was investigated. The influence

Table 4.3: Measured pH of chitosan solutions in Eu(III) kinetics experiment.

Time	D		C	
(h)	dry	pre-wet	dry	pre-wet
0	5.00	5.00	5.00	5.00
3	6.89	6.92	6.78	6.80
6	7.03	6.95	6.81	6.76
24	6.84	6.97	6.87	6.90
72	7.11	7.06	6.74	6.75

of agitation can also aid in determining the order of kinetics of the system [28]. As evident from Figure 4.8, a larger sorption capacity was observed for agitated chitosan relative to non-agitated chitosan. A similar dependence of uptake on agitation has been observed by Evans et al. for cadmium sorption on chitosan; these authors note this has also been observed by other authors [19]. Agitation was obtained by using a magnetic stir bar in the sorption vial. Agitation of the sample allowed more chitosan particles to come in contact with the solution, thus resulting in the greater sorption capacity and uptake. In contrast, when not agitated, fewer chitosan particles were in direct contact with the uranyl solution, as the powder tended to settle and clump, resulting in some of the chitosan being less accessible to UO_2^{2+} in solution. This further supports the hypothesis that sorption occurs on the surface of the chitosan particle and depends on the specific surface area, as the non-agitated chitosan effectively has a smaller specific surface area resulting from the settling and clumping effects of the unstirred sorbent.

4.1.3 Effect of initial metal concentration

The sorption isotherms for Co(II) and Eu(III) on chitosan were determined by varying the initial metal concentration. For U(VI), isotherms were determined by varying the initial sorbent concentration. For Co(II), Eu(III) and U(VI), the highest sorption capacities were observed for powder (type D) chitosan.

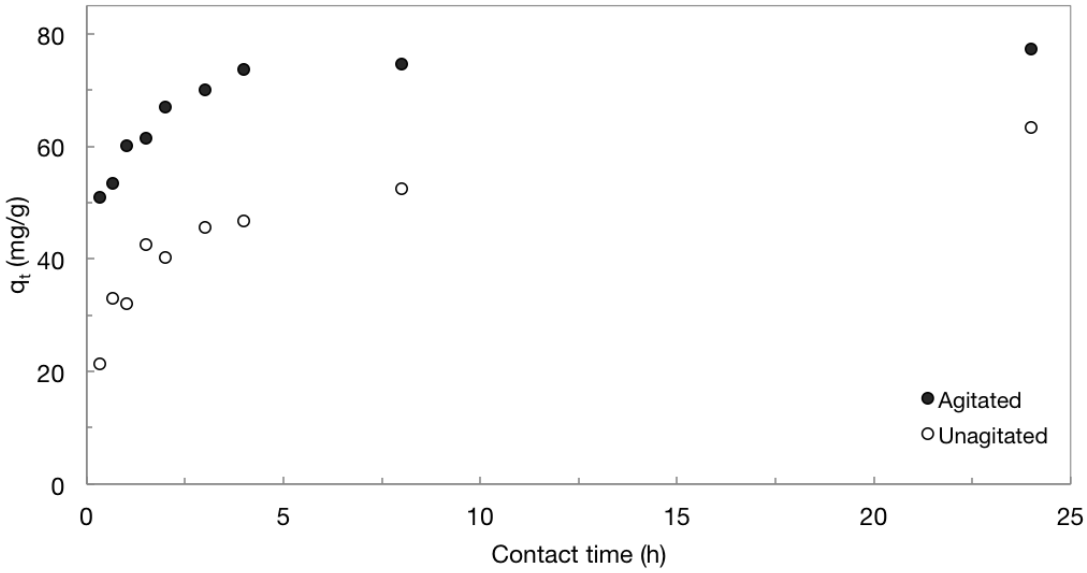

Figure 4.8: Effect of agitation on sorption kinetics of chitosan, with 2 g/L chitosan D, 200 mg/L UO_2^{2+}, initial pH = 4.6 and T = 20 °C.

4.1.3.1 Uranyl

The effect of sorbent concentration on sorption and the distribution coefficient (K_d) was examined at an initial UO_2^{2+} concentration of 200 mg/L, initial pH = 4.6, T = 20°C, and 1 hour contact time for chitosan D. As can be seen in Figure 4.9, K_d increased monotonically with increasing sorbent concentration. The increase in K_d is due to the increase accessible active sites of chitosan, with the most accessible active sites being on the surface of the chitosan powder.

The effect of sorbent concentration and initial uranyl concentration on K_d was also examined for all five chitosan types. As shown in Figure 4.10, for a given uranyl concentration, K_d increased with increasing chitosan concentration (within error). Additionally, the powder type chitosans, B, D, and E have larger changes in K_d under varying sorbent and uranyl concentrations than the flake type chitosans A and C. This is consistent with sorption occurring primarily on the surface-accessible sites: for the flake type chitosan, an increase in sorbent concentration does not result in as large of as increase in accessible active sites relative to a corresponding increase in sorbent

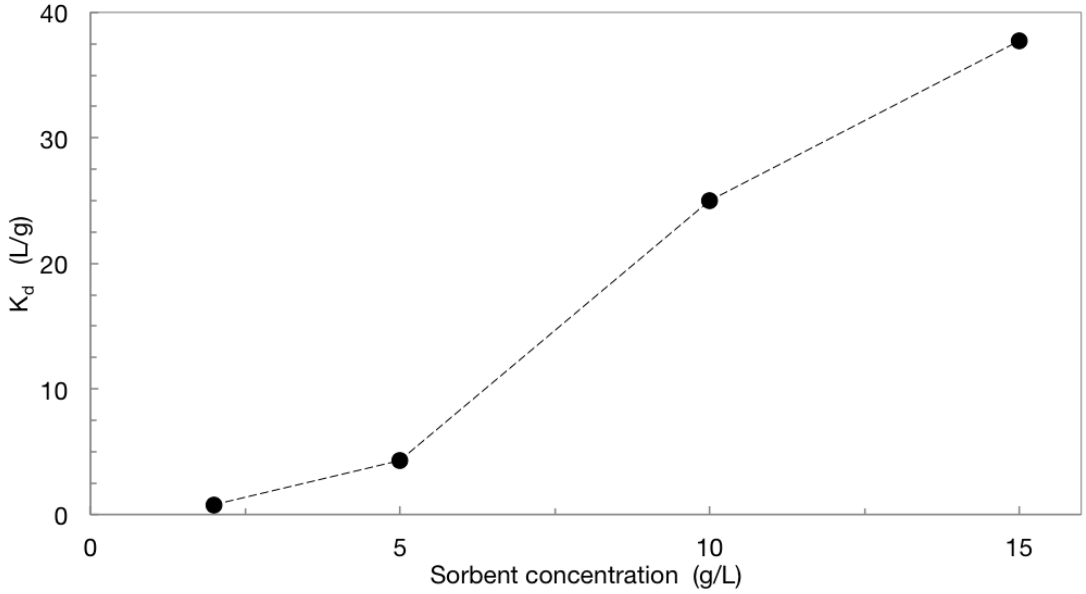

Figure 4.9: Distribution coefficient (K_d) as a function of sorbent concentration, for an initial UO_2^{2+} concentration of 200 mg/L and chitosan D.

concentration of the powder type chitosans.

The effect of sorbent concentration is also observed with respect to the residual metal concentration over time. Figure 4.11 shows the residual UO_2^{2+} concentration as a function of contact time with powder chitosan concentrations from 2–15 g/L and initial UO_2^{2+} concentration 200 mg/L. It is observed that 10 g/L chitosan is sufficient to completely[2] sorb this concentration of uranium in less than one hour, and that 5 g/L chitosan completely sorbs the uranium in six hours. A similar trend is observed for the flake-type chitosan, as shown in Figure 4.12. For the flake type chitosan, a significant decrease in UO_2^{2+} concentration between 8 and 24 hours is observed. This may be due to (a) the slow hydration kinetics of the flake-type chitosan, or (b) the hydrolysis of UO_2^{2+} into insoluble hydroxides, resulting in the removal of uranium in solution. If, as hypothesized by Piron, uranyl can only be sorbed by chitosan when the polymer is fully hydrated, then the increase in sorption after 24 hours may be attributed to the hydration of the polymer, which proceeds more slowly for the flake

[2]Within detection limits.

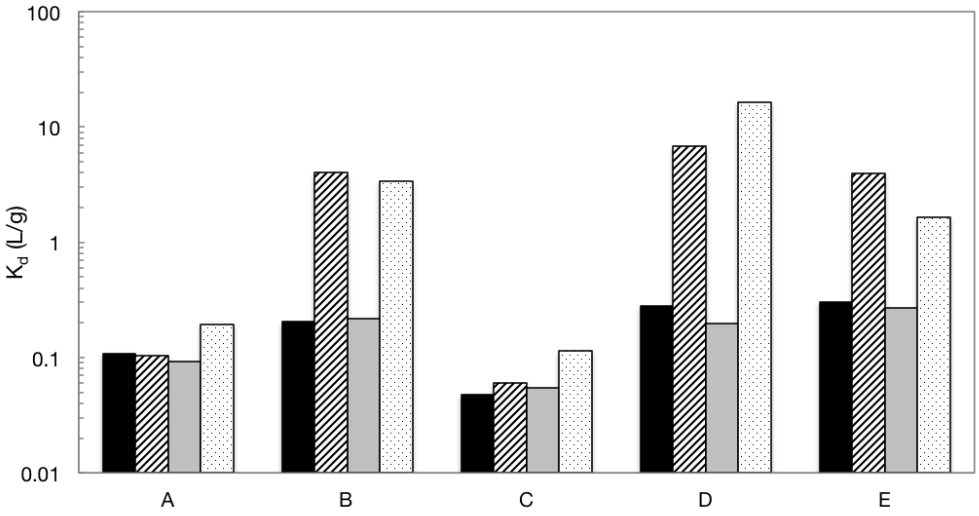

Figure 4.10: Distribution coefficient (K_d) as a function of UO_2^{2+} and sorbent concentration for chitosans A – E. Conditions: 10 minute contact time, initial pH = 4.6, T = 20°C, with 200 mg/L U and 2.5 g/L chitosan (black), 200 mg/L U and 25 g/L chitosan (striped), 2,000 mg/L U and 2.5 g/L chitosan (gray) and 2,000 mg/L U and 25 g/L chitosan (dots).

type than the powder type chitosan [64]. To account for any loss of UO_2^{2+} from solution, a control sample, containing no chitosan, was sampled at intervals to verify the absence of uranyl precipitation. However, the pH of the uranium control was not always identical to the pH of the chitosan containing samples, as it was observed that the pH of chitosan containing solutions increased with time, as shown in Figure 4.13. The increase in pH is explained by the chitosan amine groups becoming protonated, thus removing protons from solution resulting in an increase in pH, an effect observed with chitosan in the absence of metal (see Figure 4.4). Thus, due to the differences in pH of the chitosan- and control-solutions, it cannot be fully verified that UO_2^{2+} hydrolysis resulting in precipitation did not occur, as uranyl hydrolysis depends on solution pH.

As seen in Figure 4.13, the pH of chitosan-uranyl solutions was observed to increase. The increase in pH appears to be a function of chitosan concentration, supporting the hypothesis that the rise in pH is due to protonation of the amine groups

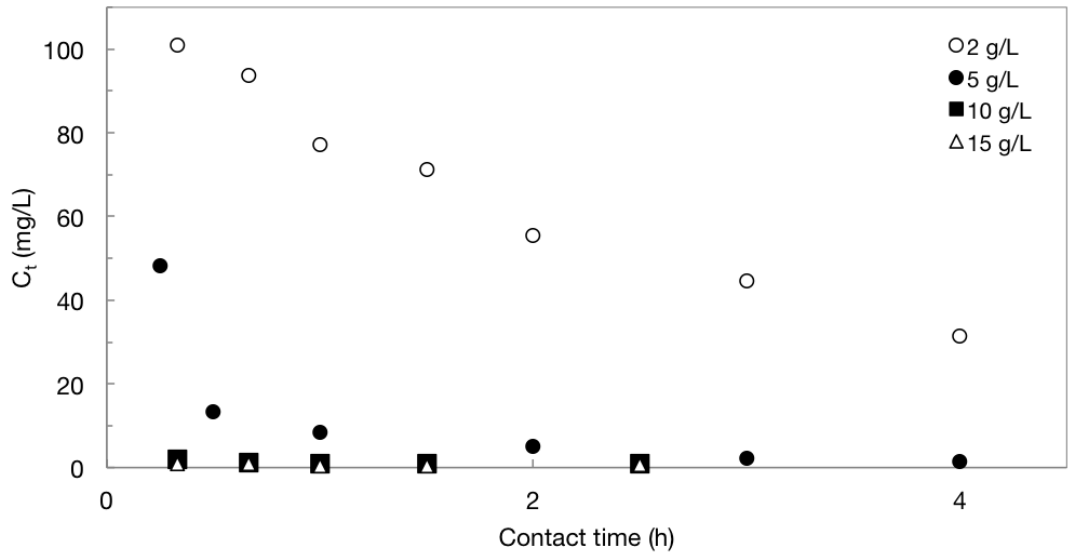

Figure 4.11: Residual UO_2^{2+} concentration as a function of time and sorbent concentration, for an initial UO_2^{2+} concentration of 200 mg/L and 2–15 g/L chitosan D.

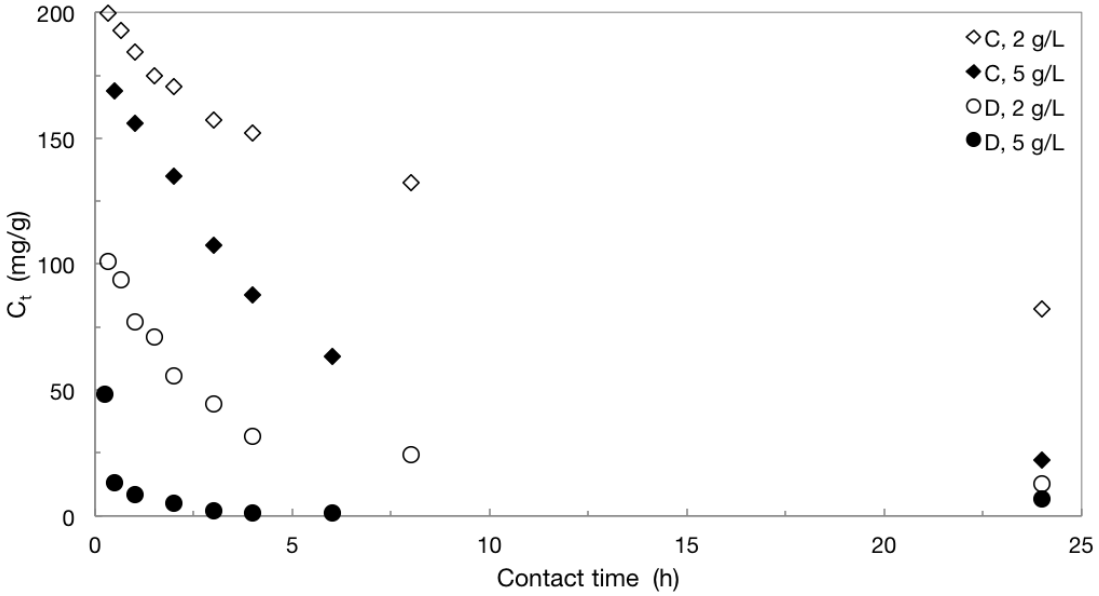

Figure 4.12: Residual UO_2^{2+} concentration as a function of time and sorbent concentration, for an initial UO_2^{2+} concentration of 200 mg/L and 2–5 g/L chitosans C and D.

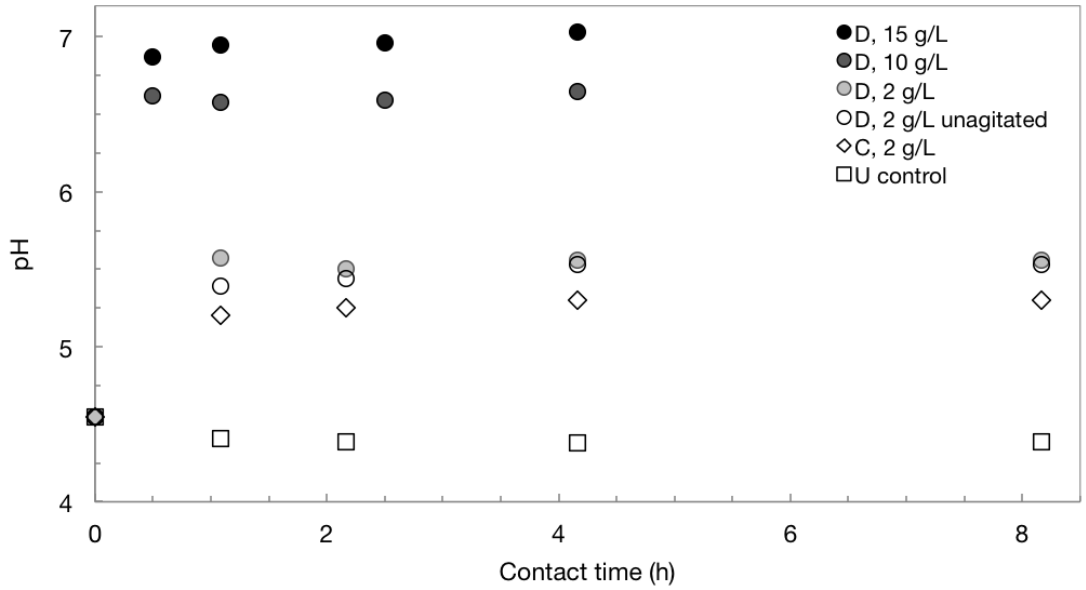

Figure 4.13: Measured pH over time of uranyl-chitosan solutions, for chitosan concentrations 0 – 15 g/L with initial pH = 4.6 and initial UO_2^{2+} concentration 200 mg/L at 20°C.

of chitosan. It is observed that a greater rise in pH is observed for the powder-type chitosan D than for an equal concentration of flake-type chitosan C. This is further evidence that there are more accessible amine groups on the powder chitosan relative to the flake chitosan. There is also an initial difference in pH change dependent on the agitation of the sample, with the pH rise in the first hour greater for an agitated solution of powder (D) chitosan relative to an unagitated solution of powder chitosan. This indicates that the hydration kinetics, as determined by protonation of amine groups, proceeds more rapidly in the agitated solution. The two solutions, agitated and non, reach equivalent pH after 4 hours, indicating that the protonation of amine groups has reached an equilibrium. It should be noted that while the pH of these two solutions reaches the same value, the sorption capacity, q_t, of both solutions sill differs, as shown in Figure 4.8.

4.1.3.2 Europium

Europium sorption capacity was determined from sorption isotherms, which were obtained by batch sorption, varying only the initial concentration of Eu(III), and using a one hour contact time. The three powder type chitosans (B, D, E) had similar sorption capacities, which were significantly greater than the adsoprtion capacities of the flake type chitosans (A, C).

The initial concentration of europium was varied from 10 to 1,000 mg·L^{-1}. As the concentration of europium increases, the pH at which Eu(III) forms insoluble $Eu(OH)_3$ decreases. At Eu concentrations in excess of 1,000 mg·L^{-1}, the dominant species (over 99%) in solution at the working pH and conditions of this experiment is the insoluble $Eu(OH)_3$, as determined by speciation diagrams produced by Medusa [69]. For this reason, initial europium concentration above 1,000 mg·L^{-1} was not used, in order to avoid the hydrolysis product $Eu(OH)_3$ and the subsequent precipitation of europium, which would invalidate the assumption of the mass balance equation which is used to determine sorbed europium. At Eu(III) concentrations less than 1,000 mg·L^{-1}, the dominant species are soluble at the pH values observed in these binding studies [69].

4.1.3.3 Cobalt

Cobalt sorption capacity was determined from sorption isotherms obtained by batch sorption by varying the initial concentration of Co(II). To determine the effect of contact time on sorption capacity, both one hour and one week (168 hour) contact times were used. Based on previous results showing the similar behavior of powder chitosan (B, D, and E) and flake chitosan (A and C), isotherm data was collected for chitosan C and D only.

The initial concentration of Co(II) was varied from 25 to 1,000 mg·L^{-1}. Due to the low activity concentration and high chemical concentration of the stock ^{60}Co, lower concentrations of cobalt could not be attained. As the concentration of cobalt increases, the pH at which Co(II) forms insoluble $Co(OH)_2$ decreases. At Co(II) concentrations of 1,000 mg·L^{-1}, and at pH 7.1, 50% of the cobalt species in solution exist as insoluble cobalt hydroxides. For comparison, at Co(II) concentrations of 100 mg·L^{-1}, and at pH

7.9, 50% of the cobalt species in solution exist as insoluble hydroxides, as determined by speciation diagrams produced by Medusa [69]. The initial pH of all cobalt solutions used for the isotherm determinations was pH = 6, which is well below the pH at which the insoluble hydroxides form. However, because chitosan raises the pH of solution as the amine groups become protonated, the pH of the chitosan-cobalt solutions increases after the initial contact. The pH of solutions was measured at the end of contact time, and in some cases, was determined to be above the threshold pH for significant formation of the insoluble cobalt hydroxide species. Isotherm data for chitosan D is not presented, as it was found that pH measured at the end of sorption exceeded the pH at which insoluble cobalt hydroxides become prevalent. Precipitated cobalt was visually observed for the highest initial cobalt concentration used, 1,000 $mg{\cdot}L^{-1}$. Consequently, this data was excluded from analysis. As in the case of europium, the precipitation of cobalt invalidates the assumptions of the mass balance equation used to determine sorption capacity.

4.1.4 Sorption mechanism of metals

While sorption of anionic species of metals on chitosan is relatively simply governed by anion-exchange mechanism and resulting in formation of ion-associate complexes with protonated aminogroups on chitosan, there is not a clear consensus on the binding mechanism(s) of cations [55], even with the large body of work on the sorption properties of chitosan toward cations.

It is generally accepted that cations of transition metals form coordination complexes with chitosan via the lone pair of electrons on the nitrogen of free (non-protonated) amine groups of chitosan, with the cationic charge of metal balanced by an anion present in solution: another ligand, organic or inorganic (e.g., carbonate, hydroxyl).

Two main models for cation binding by chitosan have been proposed in the literature: the pendant and bridge models [1, 59, 67, 73]. In the pendant model, the metal forms a complex with one amine group and hangs on the chitosan polymer chain like a pendant. In the bridge model, a cation is complexed via coordination with

multiple amine groups; the amine groups involved in the complex may be on the same polymer chain or on different polymer chains.

It has also been proposed in the literature that the hydroxyl groups on chitosan may contribute to complexation [49, 95]. Onsoyen and Skaugrud propose that the dominant Cu-chitosan complex contains two hydroxyl groups, an amine group, and either a water molecule or another hydroxyl group [60].

Some authors have used FTIR to determine the nature of chitosan-metal complexes. From FTIR spectra of chitosan contacted with uranyl, Piron and Domard observed splitting of the amide band, attributed to uranyl complexation with the nitrogen [67]. These authors further propose the formation of a neutral complex of uranyl with the amine group, which they name a pendant structure. In their proposed complex, charge is balanced by two (free) hydroxyls and water, or by two (free) hydroxyls and one hydroxyl from the chitosan polymer. The role of nitrate as a counter-ion to balance charge was dismissed, as the authors did not detect nitrate in the chitosan-uranyl complex. The authors also assume the complex is formed with UO_2^{2+}, and not the many hydrolyzed uranyl species (such as $(UO_2)_3(OH)_5^+$) also present in solution, due to (a) the steric hindrances of the polynuclear hydrolyzed species and (b) due to the observed high stability of the uranyl-chitosan complex, as determined by desorption experiments.

The FTIR spectra of chitosan after contact with UO_2^{2+} and Co(II) are shown in Figures 4.14 to 4.17. In these figures, the spectra of the chitosan contacted with metal are overlayed with the spectra of the metal solution (in nitrate or perchlorate media) and of chitosan contacted with a reference solution (nitrate or perchlorate media).

As can be seen in Figures 4.14 to 4.17, changes are observed in the spectra before and after contact with the metal solution. The band at 1590 cm^{-1} (NH_2) present in chitosan disappears after uranyl contact; it is possible that this peak is shifted to the new peak at 1522 cm^{-1} in the uranyl-chitosan spectrum. In the uranyl-contacted chitosan, the bands at 1420 (CH_2 bending), 1374 (C-H bending), 1320 (Amide III) and 1260 cm^{-1} (C-O-C stretching), which are present in the reference chitosan, are not dis-

tinct in the uranyl-contacted chitosan, as there is a broad band from around 1420 to 1250 cm^{-1} in uranyl-conatcted chitosan. This new broad band may be a nitrate band. While all uranyl experiments were done in perchloric media, the presence of nitrate is explained by the residual nitrate present from the uranyl nitrate used to prepare the uranium stock. The exaggerated presence of nitrate in the uranyl-chitosan spectra relative to the uranyl spectra indicates that nitrate is concentrated on the chitosan: either the nitrate is sorbed by chitosan [12] or is involved in the uranyl-chitosan complex. The pronounced band at 1025 cm^{-1} (C-O-C stretching) becomes a very small peak, shifted slightly to 1033 cm^{-1} after contact with uranyl. The uranyl-chitsoan spectra also gives rise to a new wide band from 920 to 890 cm^{-1}, under which the chitosan band at 894 cm^{-1} (C-O-C bridge) is not visible. Finally, there is the appearance of a new band at 823 cm^{-1} in the uranyl-chitosan spectrum. These changes in the spectra suggest that the mechanism of uranyl sorption is of a chemical nature. Although not all of the observed shifts and changes involve the NH_2 group, where complexation is suspected to take place, a complexation at that site may affect the vibrational modes of the rest of the polymer, resulting in band shifts.

Similar changes are observed in the spectrum of chitosan after contact with cobalt. The band at 1590 cm^{-1} (NH_2) disappears completely in the cobalt-chitosan spectrum, and the four bands from 1420 to 1260 are masked by the wide nitrate band present in both the cobalt-chitosan spectrum and the cobalt spectrum. Nitrate is present as cobalt was used in nitrate media. The nitrate band in the cobalt-chitosan spectrum appears slightly shifted is wider than in the cobalt-only spectrum. The nitrate band in the chitosan spectra could be the result of the nitrate band superimposed on the chitosan bands, in which case it may not actually be shifted. The three bands between 1070 to 1020 cm^{-1} are observed to shift, corresponding to C-O-C (ring) stretching. A new band is observed in the cobalt-chitosan spectrum at 1112 cm^{-1} as well as the new band at 823 cm^{-1} which was also observed in the uranyl-chitosan spectrum.

The spectra shown here were chitsoan-metal samples which were allowed to dry in open atmoshphere. FTIR spectra were also taken of cobalt-contacted chitosan after

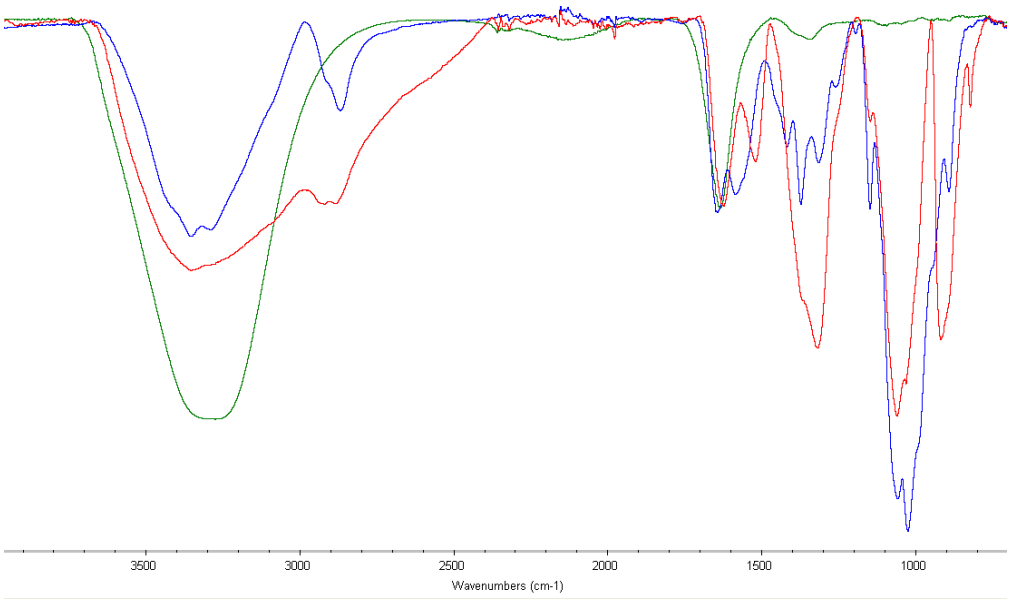

Figure 4.14: FTIR spectra of chitosan (blue), chitosan after contact with uranyl (red) and uranyl solution (green).

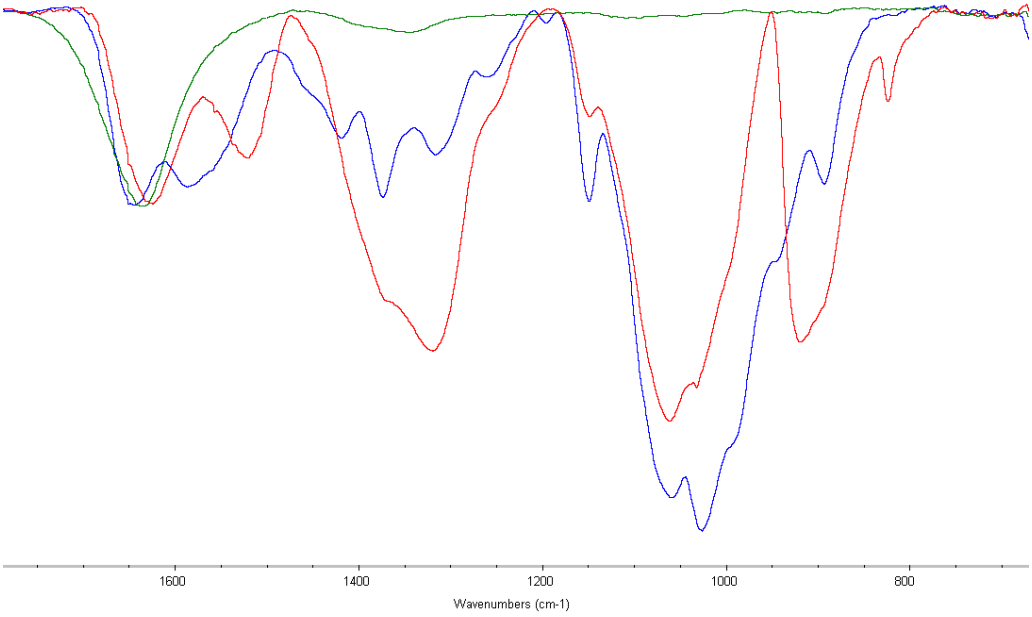

Figure 4.15: Detail of FTIR spectra of chitosan (blue), chitosan after contact with uranyl (red) and uranyl solution (green).

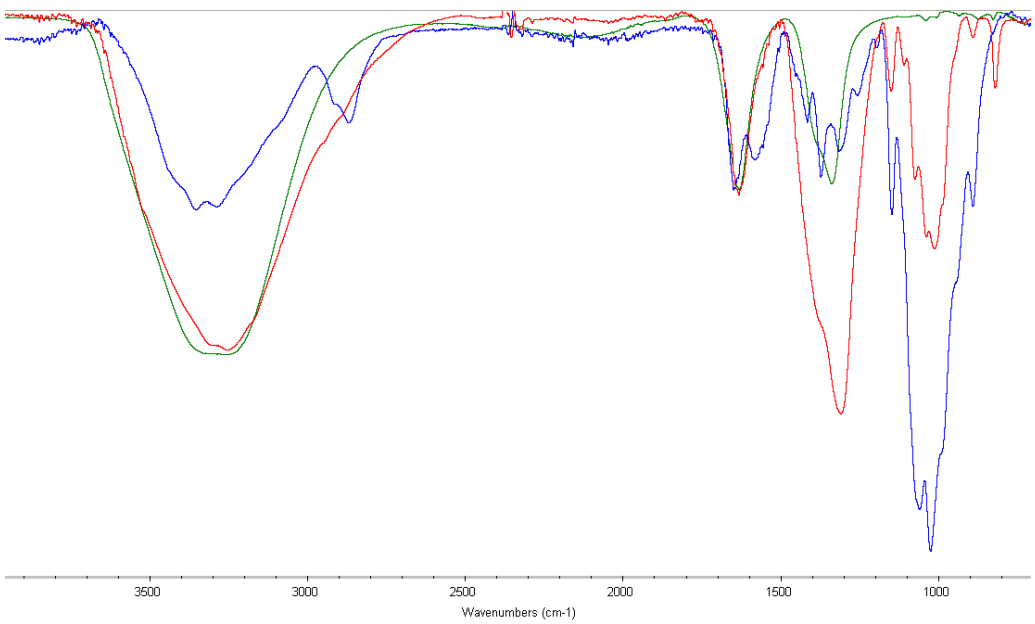

Figure 4.16: FTIR spectra of chitosan (blue), chitosan after contact with cobalt (red) and cobalt nitrate solution (green).

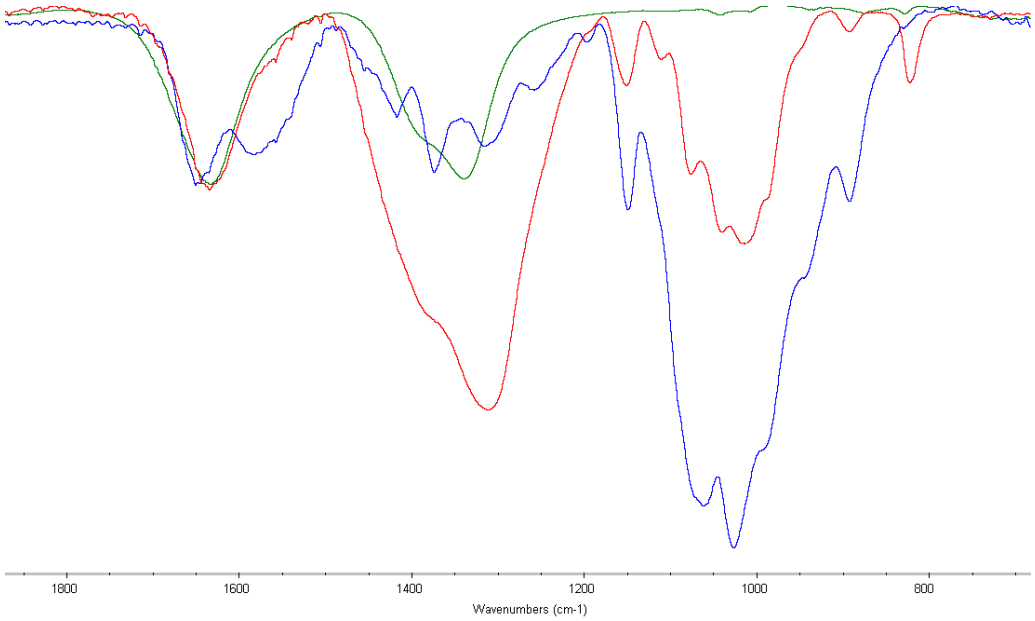

Figure 4.17: Detail of FTIR spectra of chitosan (blue), chitosan after contact with cobalt (red) and cobalt nitrate solution (green).

being dried in a desiccator and after being dried in an oven, in order to remove the water band that overlaps the N-H bending band around 1620 cm^{-1}. There were no significant changes between the spectra of the air-dried, oven-dried and desiccated samples, with the exception of the disappearance of the band at 823 cm^{-1} in the oven-dried and desiccated samples. This suggests that the band at 823 cm^{-1} may be related to water-coordiation in the complex.

4.2 Modeling sorption kinetics

A study of the kinetics of a sorption system is necessary to determine the rate-limiting step (or steps) of sorption and the kinetic parameters. These parameters are necessary for implementation of a large-scale sorption system [51]. To find these kinetic parameters, the kinetic mechanism must be determined by fitting the data to kinetic models [92]. To determine the rate limiting step(s) of cation sorption on chitosan, the pseudo-first order, pseudo-second order, intraparticle diffusion, and Elovich kinetic models were evaluated, as these are the kinetic models most applicable for biosorption systems [28]. The models were fitted by non-linear least squares regression using the statistical package R [70]. An exception is the intraparticle diffusion model, which was fitted using ordinary least squares linear regression. For comparison purposes, some of the data were also fitted using linear regression, using the common linearizations of the pseudo- first and second order and kinetic models.

Non-linear least squares regression was used preferably, as this method has been shown to be more robust than simple linear regression in the presence of both homoskedastic and heteroskedastic error distributions [18, 29, 40, 44, 45]. To evaluate the linear and nonlinear models, measures of goodness-of-fit (R^2, SSE, and RMSE), Q-Q plots and Tukey-Anscombe plots were evaluated as qualitative model diagnostics. The Tukey-Anscome and Q-Q plots for some fits of the data using linearizations of the kinetic models suggest that basic assumptions of linear regression may be violated, in particular, that the residuals may not be normally distributed after the transformation. However, given the limited number of observations in each kinetic experiment, it is

impossible to verify that the assumptions are violated or not.

Additionally, non-linear regression was used preferably because in some cases, non-realistic parameter estimates (e.g., negative rate constants) were obtained when fitting the data using linearizations of the kinetic equations with some data sets, whereas non-linear regression resulted in realistic parameter estimates. It was observed that the parameter estimates from linearizations of kinetic equations were more sensitive to variations in the data, as well as outliers, relative to the non-linear method. For example, the linear fit of the pseduo-second order equation, using the full data of the europium sorption kinetics of un-wet powder chitosan results in a negative value for the rate constant k_2, even though the model appears to fit well with a $R^2 = 0.99995$. When the observation at 168 h is removed, the model results in a positive rate constant. This issue does not arise when the non-linear method is used. To eliminate this issue and others associated with linearizations, the non-linear method was used for all analyses and reported parameter estimates.

4.2.1 Effect of particle size

Particle size has been found to have an effect on sorption kinetics in chitosan-metal biosorption systems by several authors [17, 19, 23, 24, 36]. Jansson-Charrier et al. found that the maximum uptake of vanadium by chitosan was a function of the specific surface area of the sorbent, with smaller particles having greater maximum sorption capacities. Dzul Erosa et al. found the same effect for chitosan sorption of cadmium. Uptake dependence on particle size has also been found for uranyl and zinc [24], but not for other cations such as copper, mercury, or nickel [51, 52]. Thus, the difference in maximum sorption capacity found between the fibrous (C) and powder (D) chitosans used here may be partially explained by their differing specific surface areas. It is important to note that in the studies cited above, fractionated portions of the same type of chitosan were compared, whereas in this work, two different chitosans (of two different particle sizes) were used. In this work, greater uptake capacity was observed for the powder chitosan relative to the fiber chitosan for cobalt, europium

and uranyl sorption.

Guibal et al. concluded that the dependence of sorption kinetics on particle size suggested that the kinetics were largely governed by intraparticle diffusion [23, 24]. If intraparticle diffusion is the rate limiting step, the sorption capacity will be linear with respect to the square root of contact time, as proposed by Weber and Morris [28]. When uranyl and europium sorption is modeled this way, two linear sections are observed, as shown in Figures 4.18 and 4.19. The different linear sections may correspond to a range of pore sizes in the sorbent, with different observed rate constants for different pore sizes [24, 28]. It can be assumed that each chitosan sorbent used contained a range of pore sizes, given the non-homogenous nature of the sorbent. McKay et al. note that it is common to observe up to four regions in a Weber-Morris plot, with up to three of them linear, resulting from diffusion into increasingly smaller pores of the sorbent [51]. Guibal et al. propose that multi-linearity in the Weber-Morris model may result from a combination of pore and surface diffusion in the sorbent [24]. It is also possible for the rate-limiting step of sorption kinetics to change during the sorption [28]. It is generally accepted that a kinetic process requiring more than 24 hours to reach equilibrium is diffusion controlled [28].

4.2.2 Intraparticle diffusion model

In order to compare the Weber-Morris intraparticle diffusion model to the other kinetic models considered, the kinetic data was broken into parts, determined by the apparent linear sections. The resulting linear fits are shown in Figures 4.18 and 4.19 and the resulting model parameters in Tables 4.4 and 4.5. From Figures 4.18 and 4.19, it is clear that two linear sections are present. Due to the limited data set, which results in one degree of freedom for each linear section for the europium data, it is impossible to provide good estimates of the error in the parameter estimates resulting from the linear fit. It should also be noted that the small data set results in values of the correlation coefficient (R^2) which are very close to unity; this is, at least in part, an artifact of the small sample size and resulting low degrees of freedom. However, it

can be determined that the intraparticle diffusion rate constant, k_d, changes between the two linear sections in all cases. The transition point for the two linear sections is at approximately 24 hours contact time for europium and around three hours for uranium. The high initial uptake rate which decreases with time is consistent with intraparticle diffusion as the rate-limiting step [19]. In all cases, the Weber-Morris plots do not pass through the origin, which can be interpreted as evidence for the existence of external film control or a boundary layer [22, 28]. The thickness of the boundary layer can be determined from the intercept of the Weber-Morris plot.

For europium sorption, the rate constants of the second linear section are more similar in the prewet and untreated samples relative to the change in rate constant for the first linear section, where the rate constants differ by nearly a factor of 2, with the larger rate constant for dry chitosan. The differing rate constant may be largely due to the intraparticle diffusion of water in the un-hydrated sorbent relative to the pre-wet sorbent. Such an effect was observed by Piron et al. for uranyl sorption on chitosan [64]. These authors found that an un-hydrated sorbent tended toward non-linear, non-Fickian behavior as the system progressed to equilibrium. It is observed that the rate constant of the un-wet system approaches the rate constant of the hydrated system in the second linear section (over 24 hour contact time) as the system approaches equilibrium. This observation is consistent with the first linear section of the un-wet sorbent corresponding to diffusion of water in the sorbent.

The effect of agitation on uranyl sorption is shown in Figure 4.19. While the overall sorption capacity is less in the unagitated solution, the rate constant is greater in the unagitated solution relative to the agitated solution in both linear sections. The rate constant of the second linear section in the agitated solution decreases more than that of the unagitated solution, which is consistent with the agitated solution attaining equilibrium before the unagitated solution. Likewise, the rate constant of the second linear section of the flake type chitosan (C) decreases less than that of the powder (D) chitosan. This reflects the additional time required for solution to diffuse through the larger flakes relative to the powder.

Increased agitation rate has been observed to both increase metal uptake [19] as well as have little effect on uptake [6, 17, 22]. In particular, Evans et al. found uptake to increase with agitation speed up to a limit, after which an increase in agitation speed had no effect on uptake. This is taken as evidence for the existence of boundary layer around the chitosan particles, with the boundary layer decreasing with agitation rate [19]. Furthermore, in a system without agitation, a concentration gradient may exist in the solution, which may result in bulk diffusion being the limiting diffusion step [22]. When external diffusion is limiting, sorption rate will be controlled by agitation speed [22].

4.2.3 Other models

The non-linear least squares parameter estimates for europium, cobalt and uranyl sorption kinetics are shown in Tables 4.6 through 4.11. Based on the R^2, RMSE, and SSE metrics, it appears that the pseudo-second order model provides a better fit than the pseudo-first order model, and that the Elovich model provides the best fit of the data. This is substantiated by visual inspection of the three model fits. For example, Figure 4.20 shows the pseudo-first order, pseudo-second order, and Elovich model fits for europium sorption on flake type chitosan (C), which is representative of fits of other europium data to these models. However, it is difficult to determine the best fitting model from the error metrics alone. While the parameters estimated by the Elovich model provide a good fit to the data, they are not all statistically significant at the 5 or 10% level. While this may be in part due to the small sample size, it may also indicate a lack of fit of the model. The 95% confidence intervals (which are denoted 2σ in the tables) of some model parameter estimates, especially in the Elovich model, are of greater magnitude than the parameter estimates and hence include zero as a parameter estimate. This suggests some lack of fit of the model in such cases. All three models underestimate the equilibrium sorption capacity, q_e, relative to the q_e determined by Langmuir and Freundlich isotherm modeling for all metals.

Based on the relative fits of the models, it is difficult to determine a single model

Table 4.4: Intraparticle diffusion model (Weber-Morris) parameter estimates for Eu(III) sorption onto chitosan C. Conditions: 50 mg/L Eu(III), pH=5, 5 g/L sorbent.

Sorbent	Linear section	k_d (mg/g· $h^{1/2}$)	C (mg/g)	R^2
C	one	1.039	1.026	0.988
	two	0.156	3.381	0.999
C, prewet	one	0.596	2.813	0.999
	two	0.128	4.351	0.996

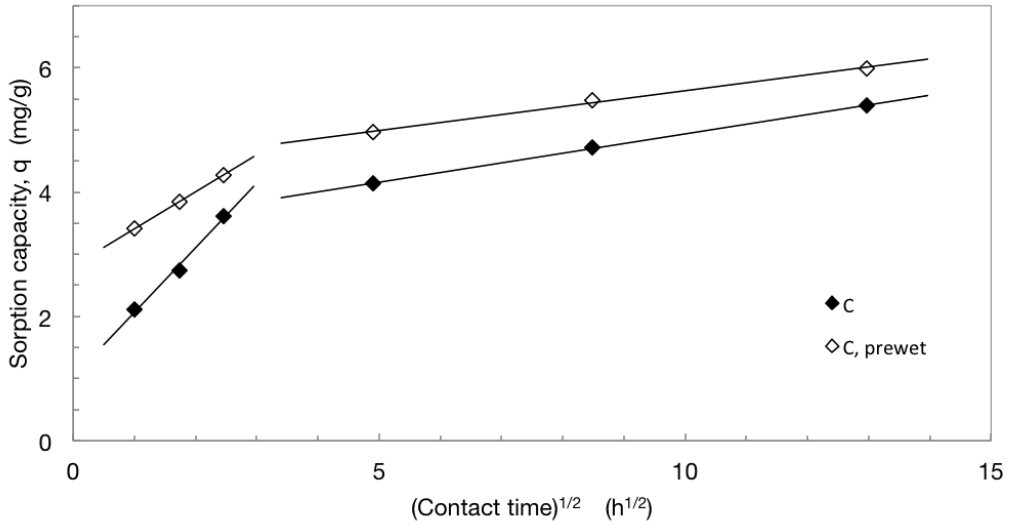

Figure 4.18: Effect of polymer hydration on europium sorption kinetics, Weber-Morris intraparticle diffusion model, for chitosan C. Conditions: 50 mg/L Eu(III), pH=5, 5 g/L sorbent.

to be "best." There may be multiple mechanisms, such as intraparticle diffusion and chemical adsorption, resulting in multiple rate-limiting steps. Such a phenomenon would likely result in relatively poor fits of models only taking one mechanism into account.

Table 4.5: Intraparticle diffusion model (Weber-Morris) parameter estimates for uranyl sorption onto chitosan. Conditions: 200 mg/L UO_2^{2+}, pH=4.6, 2 g/L sorbent.

Sorbent	Linear section	k_d (mg/g· $h^{1/2}$)	C (mg/g)	R^2
D, agitated	one	17.4	40.9	0.962
	two	1.2	71.3	0.998
D, unagitated	one	23.1	10.7	0.841
	two	5.6	35.9	0.995
C, agitated	one	15.4	-8.7	0.986
	two	8.4	2.4	0.999

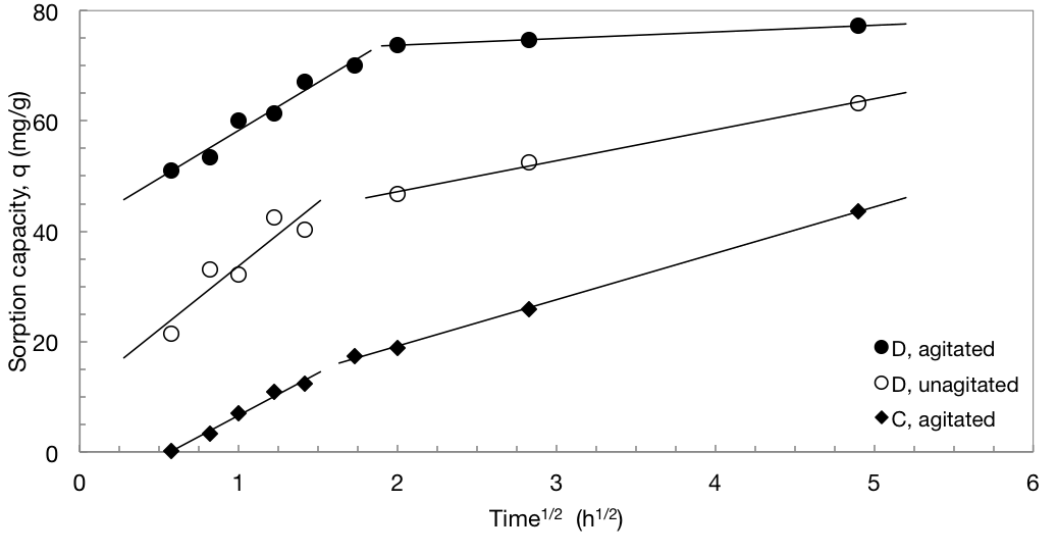

Figure 4.19: Effect of agitation and sorbent type on uranyl sorption kinetics, Weber-Morris intraparticle diffusion model, for chitosan C and D. Conditions: 200 mg/L UO_2^{2+}, pH=4.6, 2 g/L sorbent.

Table 4.6: Kinetic model parameter estimates for Eu(III) sorption onto chitosan, estimated by non-linear least squares.

Sorbent	Pseudo-first order				
	$k_1 \pm 2\sigma$ (h^{-1})	$q_e \pm 2\sigma$ (mg/g)	RMSE	SSE	R^2
C	0.33 ± 0.29 ($*$)	4.66 ± 1.01 ($*$)	0.64	0.19	0.78
C, prewet	0.84 ± 0.99 ($\circ$)	5.07 ± 1.10 ($*$)	0.80	0.85	0.01
D	2.73 ± 2.28 ($*$)	6.91 ± 0.42 ($*$)	0.34	0.01	0.26
D, prewet	3.60 ± 1.38 ($*$)	7.05 ± 0.11 ($*$)	0.09	6.2E-4	0.50
	Pseudo-second order				
	$k_2 \pm 2\sigma$ (g mg^{-1} h^{-1})	$q_e \pm 2\sigma$ (mg/g)	RMSE	SSE	R^2
C	0.10 ± 0.09($*$)	4.92 ± 0.77($*$)	0.43	0.07	0.90
C, prewet	0.22 ± 0.24 ($\circ$)	5.42 ± 0.83 ($*$)	0.51	4.91	0.79
D	1.24 ± 1.57 ($\circ$)	7.03 ± 0.37 ($*$)	0.25	0.63	0.59
D, prewet	3.72 ± 2.70 ($*$)	7.09 ± 0.08($*$)	0.06	2.5E-4	0.80
	Elovich				
	$a \pm 2\sigma$ (units)	$b \pm 2\sigma$ (units)	RMSE	SSE	R^2
C	20.6 ± 22.7 ($\circ$)	1.61 ± 0.33 ($*$)	0.19	1.3E-2	0.98
C, prewet	385.1 ± 229.5($*$)	1.98 ± 0.14 ($*$)	0.06	7.5E-4	1.00
D	2.02E17 $\pm$ 7.4E18	6.48 ± 5.48 ($*$)	0.21	3.6E-3	0.73
D, prewet	1.41E52 $\pm$ 3.6E53	17.89 ± 3.67 ($*$)	0.02	2.7E-5	0.98

($*$) indicates the parameter estimate is statistically significant with $p < 0.05$.
($\circ$) indicates the parameter estimate is statistically significant with $0.05 < p < 0.1$.

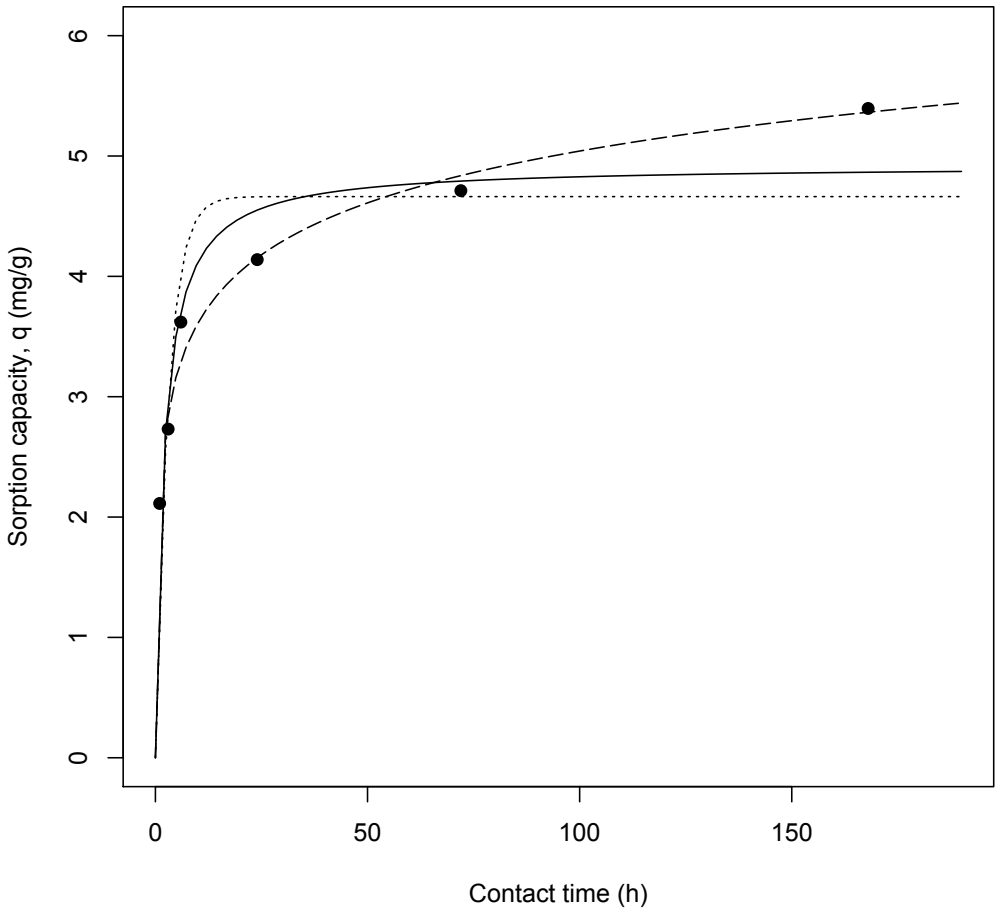

Figure 4.20: Pseudo-first oder (dotted), pseudo-second order (solid) and Elovich (dashed) kinetic models fit by NLLS for Eu(III) sorption by chitosan C, with 5 g/L chitosan and Eu(III) concentration 50 mg/L.

Table 4.7: Effect of initial Co(II) concentration on kinetic model parameter estimates for Co(II) sorption onto chitosan, estimated by non-linear least squares. Conditions: 5 g/L chitosan D, initial pH = 6, T = 37°C.

	Pseudo-first order				
$[Co^{2+}]$ (mg/L)	$k_1 \pm 2\sigma$ (h^{-1})	$q_e \pm 2\sigma$ (mg/g)	RMSE	SSE	R^2
50	3.94 ± 3.0 *	3.36 ± 0.34 *	0.41	0.140	0.22
100	3.26 ± 2.3 *	5.82 ± 0.74 *	0.81	0.189	0.49
200	4.88 ± 3.0 *	9.77 ± 0.99 *	0.96	0.069	0.49
	Pseudo-second order				
$[Co^{2+}]$	$k_2 \pm 2\sigma$ (g mg^{-1} h^{-1})	$q_e \pm 2\sigma$ (mg/g)	RMSE	SSE	R^2
50	1.58 ± 1.2 *	3.61 ± 0.31 *	0.28	0.068	0.64
100	0.73 ± 0.5 *	6.19 ± 0.59 *	0.55	0.093	0.77
200	0.86 ± 0.6 *	10.3 ± 0.82 *	0.62	0.030	0.78
	Elovich				
$[Co^{2+}]$	$a \pm 2\sigma$	$b \pm 2\sigma$	RMSE	SSE	R^2
50	1.77 E4 $\pm$ 5.1E4	3.76 ± 1.09 *	0.14	0.019	0.91
100	4.74E3 $\pm$ 1.2E4	1.96 ± 0.49 *	0.31	0.025	0.92
200	1.62E6 $\pm$ 1.6E7	1.68 ± 0.12 *	0.75	0.034	0.69

(*) indicates the parameter estimate is statistically significant with $p < 0.05$.
2σ values calculated from error in parameter estimates only.

Table 4.8: Effect of initial pH and sorbent type on kinetic model parameter estimates for Co(II) sorption onto chitosan, estimated by non-linear least squares. Conditions: 10 g/L chitosan, [Co] = 50 mg/L, T = 37°C. Initial pH=6, except for D′, where initial pH=4.6.

Sorbent	Pseudo-first order				
	$k_1 \pm 2\sigma$ (h^{-1})	$q_e \pm 2\sigma$ (mg/g)	RMSE	SSE	R^2
C	1.10 ± 0.4 *	1.75 ± 0.16 *	0.15	0.157	0.86
D	5.67 ± 2.8 *	3.04 ± 0.15 *	0.18	0.029	0.36
D′	4.11 ± 1.9 *	2.64 ± 0.16 *	0.20	0.045	0.49
	Pseudo-second order				
	$k_2 \pm 2\sigma$ (g mg^{-1} h^{-1})	$q_e \pm 2\sigma$ (mg/g)	RMSE	SSE	R^2
C	0.86 ± 0.2 *	1.90 ± 0.08 *	0.06	0.030	0.98
D	3.80 ± 2.0 *	3.16 ± 0.11 *	0.11	0.011	0.77
D′	2.71 ± 1.2 *	2.78 ± 0.12 *	0.11	0.014	0.84
	Elovich				
	$a \pm 2\sigma$	$b \pm 2\sigma$	RMSE	SSE	R^2
C	40.51 ± 61	4.37 ± 19.37 *	0.13	0.076	0.90
D	1.72E8 $\pm$ 4.0E8	7.39 ± 0.81 *	0.03	0.001	0.98
D′	4.19E5 $\pm$ 1.0E6	6.23 ± 0.10 *	0.05	0.004	0.96

(*) indicates the parameter estimate is statistically significant with $p < 0.05$.
2σ values calculated from error in parameter estimates only.

Table 4.9: Effect of temperature on kinetic model parameter estimates for Co(II) sorption onto chitosan, estimated by non-linear least squares. Conditions: 5 g/L chitosan D, [Co] = 50 mg/L, initial pH=6.

T (°C)	Pseudo-first order				
	$k_1 \pm 2\sigma$ (h^{-1})	$q_e \pm 2\sigma$ (mg/g)	RMSE	SSE	R^2
20	2.49 ± 1.0 *	4.32 ± 0.28 *	0.37	0.098	0.63
37	3.94 ± 2.9 *	3.36 ± 0.33 *	0.41	0.140	0.22
	Pseudo-second order				
	$k_2 \pm 2\sigma$ (g mg^{-1} h^{-1})	$q_e \pm 2\sigma$ (mg/g)	RMSE	SSE	R^2
20	0.95 ± 0.3 *	4.55 ± 0.17 *	0.19	0.028	0.90
37	1.58 ± 1.2 *	3.61 ± 0.30 *	0.28	0.068	0.64
	Elovich				
	$a \pm 2\sigma$	$b \pm 2\sigma$	RMSE	SSE	R^2
20	1.03E5 $\pm$ 3.5E5	3.56 ± 0.88 *	0.20	0.031	0.97
37	1.77E4 $\pm$ 4.9E4	3.76 ± 1.05 *	0.14	0.019	0.91

(*) indicates the parameter estimate is statistically significant with $p < 0.05$.
2σ values calculated from error in parameter estimates only.

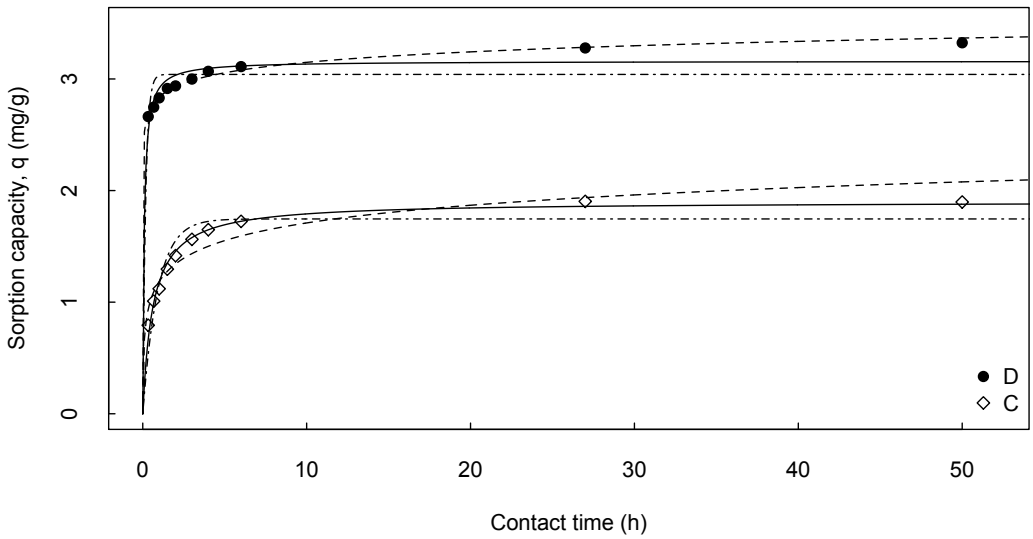

Figure 4.21: Pseudo-first order (dot-dash), pseudo-second order (solid) and Elovich (dashed) kinetic models fit by NLLS for Co(II) sorption by chitosan C (diamonds) and D (circles). Conditions: 10 g/L chitosan, $[Co^{2+}]$ = 50 mg/L, pH = 6, at 37°C.

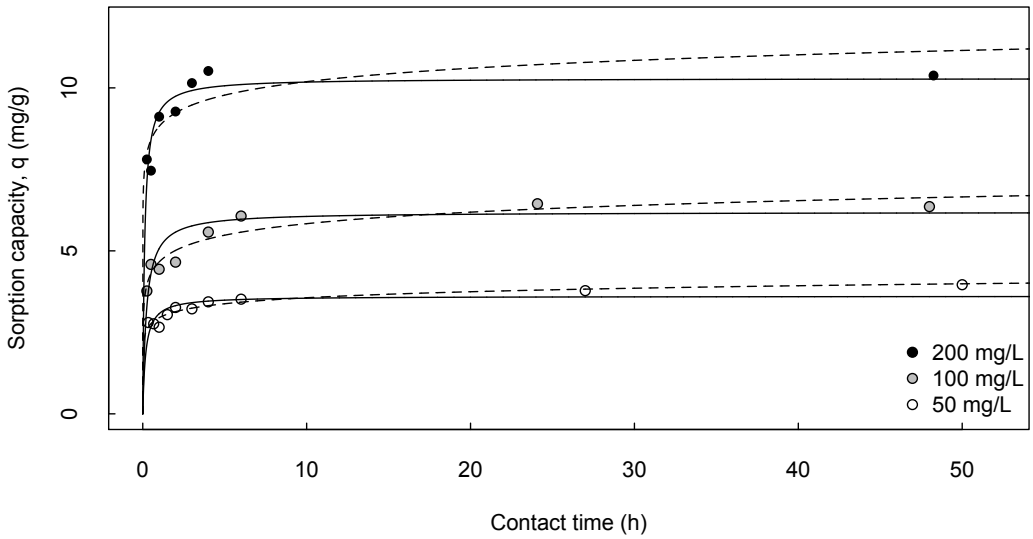

Figure 4.22: Effect of initial metal concentration on sorption kinetics: pseudo-second order (solid) and Elovich (dashed) kinetic models fit by NLLS for Co(II) sorption by chitosan D. Conditions: 5 g/L chitosan, $[Co^{2+}]$ = 50 mg/L (empty circles), 100 mg/L (gray circles) or 200 mg/L (black circles), pH = 6, at 37°C.

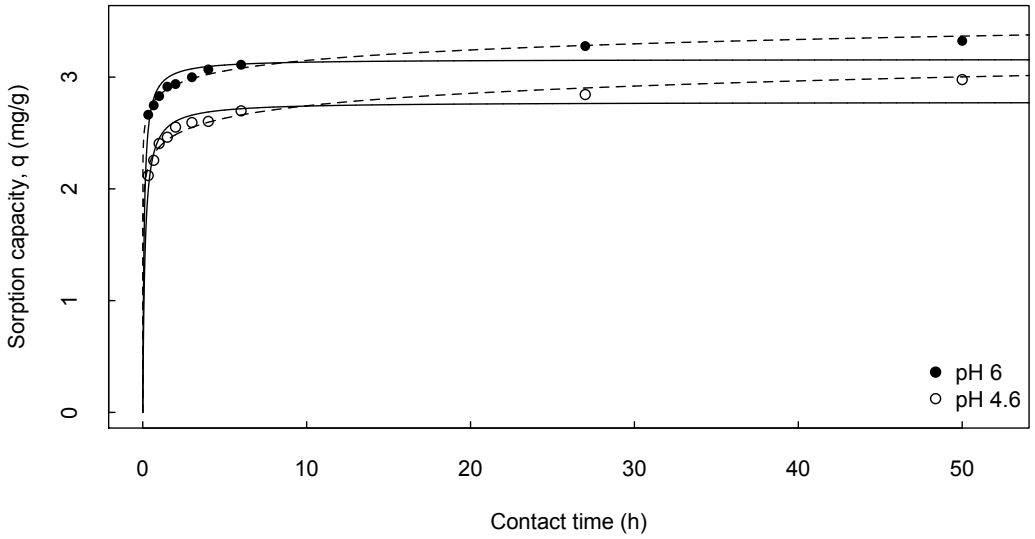

Figure 4.23: Effect of initial pH on sorption kinetics: pseudo-second order (solid) and Elovich (dashed) kinetic models fit by NLLS for Co(II) sorption by chitosan D. Conditions: 10 g/L chitosan, $[Co^{2+}]$ = 50 mg/L, pH = 6 (solid circles) or pH= 4.6 (empty circles), at 37°C.

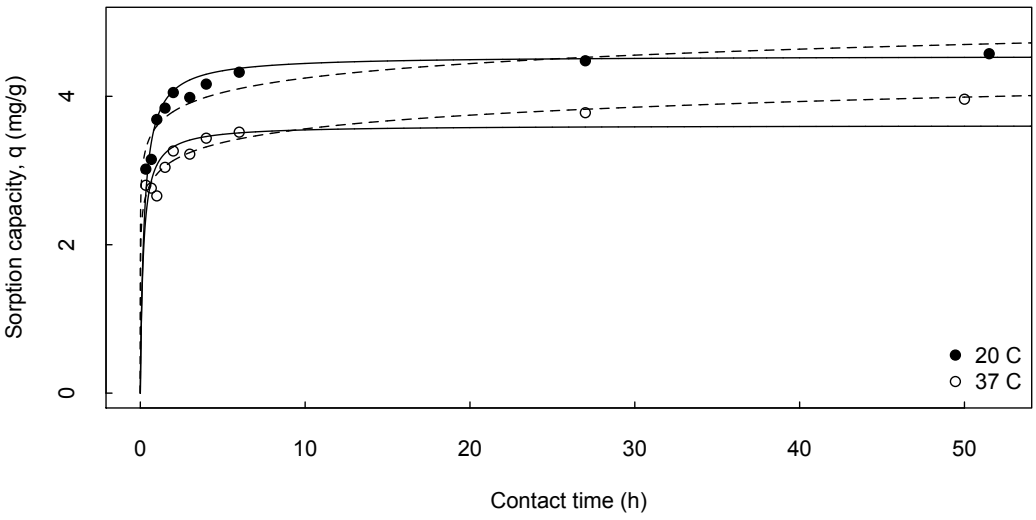

Figure 4.24: Effect of temperature on sorption kinetics: pseudo-second order (solid) and Elovich (dashed) kinetic models fit by NLLS for Co(II) sorption by chitosan D. Conditions: 5 g/L chitosan, $[Co^{2+}]$ = 50 mg/L, pH = 6, at 20°C or 37 °C.

Table 4.10: Kinetic model parameter estimates for uranyl sorption onto chitosan, estimated by non-linear least squares. Conditions: 200 mg/L UO_2^{2+}, initial pH=4.6, T = 20°C, 2 or 5 g/L chitosan C, D.

Sorbent	Loading	Pseudo-first order				
	(g/L)	$k_1 \pm 2\sigma$ (h^{-1})	$q_e \pm 2\sigma$ (mg/g)	RMSE	SSE	R^2
C	2	0.141 ± 0.04 *	44.0 ± 6.51 *	2.25	156.8	0.97
	5	0.279 ± 0.05 *	27.2 ± 1.72 *	1.05	0.161	0.99
D	2	2.779 ± 1.39 *	70.1 ± 6.26 *	6.44	0.081	0.59
	5	6.158 ± 0.72 *	38.3 ± 0.55 *	0.63	0.002	0.96
		Pseudo-second order				
		$k_2 \pm 2\sigma$ (g mg^{-1} h^{-1})	$q_e \pm 2\sigma$ (mg/g)	RMSE	SSE	R^2
C	2	0.002 ± 0.001 *	56.7 ± 9.03 *	1.76	209.2	0.98
	5	0.012 ± 0.003 *	29.9 ± 1.86 *	0.88	0.056	0.99
D	2	0.060 ± 0.27 *	75.5 ± 4.43 *	3.34	0.024	0.89
	5	0.432 ± 0.22 *	39.0 ± 1.31 *	1.26	0.009	0.82
		Elovich				
		$a \pm 2\sigma$	$b \pm 2\sigma$	RMSE	SSE	R^2
C	2	8.76 ± 2.1 *	0.060 ± 0.01 *	1.52	287.2	0.99
	5	24.4 ± 18.3 *	0.178 ± 0.05 *	1.99	0.131	0.95
D	2	4E4 $\pm$ 1.0E5	0.145 ± 0.04 *	3.13	0.015	0.90
	5	1.9E17 $\pm$ 1E19	1.10 ± 1.48	2.49	0.040	0.31

(*) indicates the parameter estimate is statistically significant with $p < 0.05$.
2σ values calculated from error in parameter estimates only.

Table 4.11: Kinetic model parameter estimates for uranyl sorption onto chitosan, estimated by non-linear least squares. Conditions: 200 mg/L UO_2^{2+}, initial pH = 4.6, T = 20°C, 2 or 5 g/L chitosan C, D.

Sorbent	Pseudo-first order				
	$k_1 \pm 2\sigma$ (h^{-1})	$q_e \pm 2\sigma$ (mg/g)	RMSE	SSE	R^2
Unagitated	1.131 ± 0.61 *	51.9 ± 7.84 *	6.29	0.171	0.77
Agitated	2.779 ± 1.39 *	70.1 ± 6.26 *	6.44	0.081	0.59
	Pseudo-second order				
	$k_2 \pm 2\sigma$ (g mg^{-1} h^{-1})	$q_e \pm 2\sigma$ (mg/g)	RMSE	SSE	R^2
Unagitated	0.025 ± 0.014 *	58.7 ± 6.66 *	3.84	0.062	0.91
Agitated	0.060 ± 0.27 *	75.5 ± 4.43 *	3.34	0.024	0.89
	Elovich				
	$a \pm 2\sigma$	$b \pm 2\sigma$	RMSE	SSE	R^2
Unagitated	361.5 ± 853.1 *	1.07E-1 $\pm$ 0.02 *	2.49	0.044	0.96
Agitated	4.0E4 $\pm$ 1.0E5	1.45E-1 $\pm$ 0.04 *	3.13	0.015	0.90

(*) indicates the parameter estimate is statistically significant with $p < 0.05$.
2σ values calculated from error in parameter estimates only.

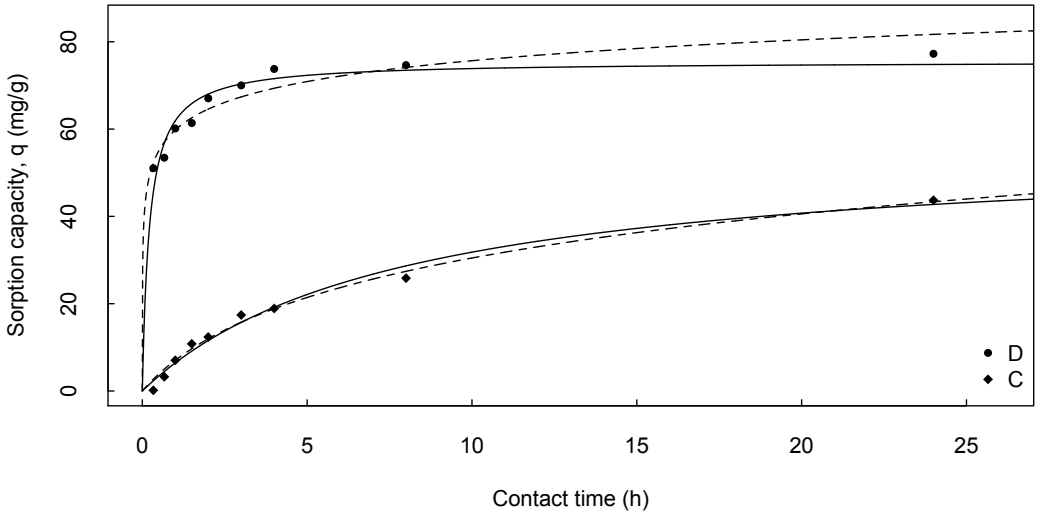

Figure 4.25: Pseudo-second order (solid) and Elovich (dashed) kinetic models fit by NLLS for uranyl sorption by chitosan C (diamonds) and D (circles). Conditions: 2 g/L chitosan, $[UO_2^{2+}]$ = 200 mg/L, pH = 4.6, at 20°C.

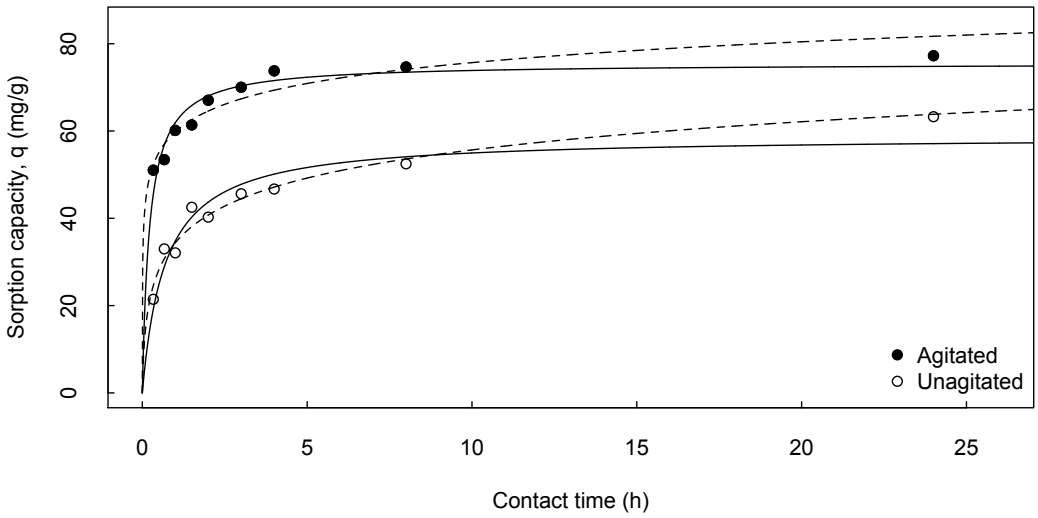

Figure 4.26: Effect of agitation on sorption kinetics: pseudo-second order (solid) and Elovich (dashed) kinetic models fit by NLLS for uranyl sorption by chitosan D. Conditions: 2 g/L chitosan, $[UO_2^{2+}]$ = 200 mg/L, pH = 4.6, at 20°C.

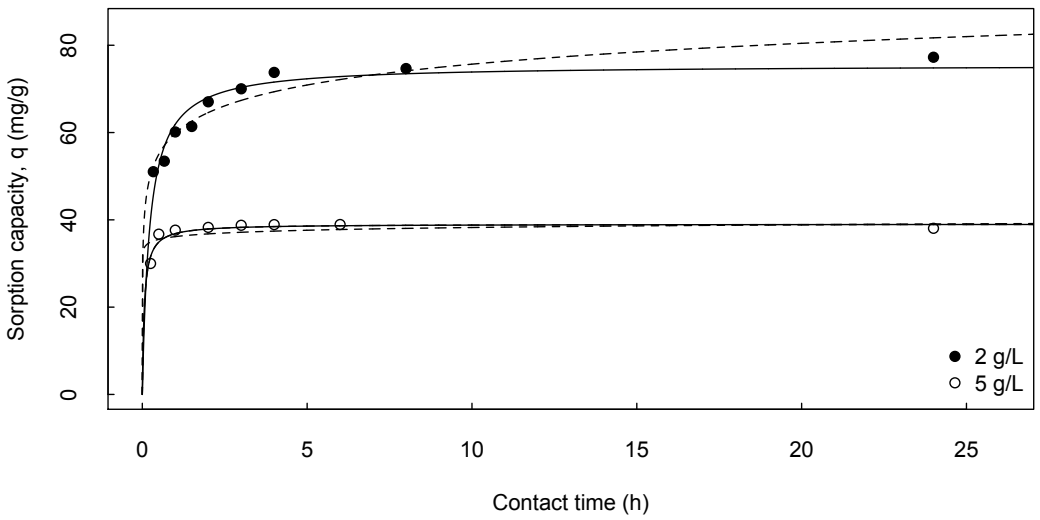

Figure 4.27: Effect of sorbent laoding on sorption kinetics: pseudo-second order (solid) and Elovich (dashed) kinetic models fit by NLLS for uranyl sorption by chitosan D. Conditions: $[UO_2^{2+}]$ = 200 mg/L, pH = 4.6, at 20°C.

4.3 Modeling sorption isotherms

The data were modeled by Langmuir and Freundlich isotherms. Isotherms were fitted to the experimental data by linear and non-linear least squares (NLLS) regression. The parameter estimates for Langmuir and Freundlich isotherms of cobalt, europium and uranyl sorption on chitosan are shown in Tables 4.13 to 4.16.

It has been found that the method of fitting experimental data to isotherm models can have a significant effect on the estimates of the model parameters [18, 43]. In this work, the data were fitted to Langmuir and Freundlich isotherms by non-linear least squares regression, and for comparison, by using ordinary least squares regression on linearized forms of the isotherms. The Langmuir isotherm is commonly linearized in four ways, each resulting in different parameter estimates, and each with a different error distribution. Importantly, the error distributions of the linearized forms of the isotherms is not identical to the error distribution of the non-linearized form of the isotherms. Additionally, the weighting of the data points changes with the linearizations [43]. Table 4.12 shows the nonlinear and linear forms of the Langmuir and Freundlich isotherms used in this analysis. To illustrate the difference in parameter estimates and resulting curve fit resulting from the different linearizaitons of the isotherms, Figure 4.28 shows the isotherms resulting from the parameters obtained by non-linear least squares and the parameters obtained by using the four linearized forms of the Langmuir isotherm equation for europium sorption on flake chitosan (C). From this figure, it appears that the nonlinear method results in the best fit of the data. Similar results were observed for the other metals on all chitosan types.

The linear forms of the isotherms presented in Table 4.12 were fit to a selection of the experimental data (chitosans C and D) in order to examine the dependence of the parameter estimates on the linearization. Types C and D were chosen as representative of the powder and flake type chitosan, respectively. Linear isotherms were fitted using ordinary least squares regression. Non-linear isotherms were fit to experimental data using an iterative Gauss-Newton algorithm in the statistical package R [70]. Langmuir and Freundlich isotherms, fit by NLLS, for europium, cobalt and uranyl sorption on

chitosan are shown in Figures 4.29, 4.30, and 4.31 respectively. The parameter estimates for these models are shown in Tables 4.13, 4.15 and 4.16.

The goodness-of-fit of the different isotherm models can be measured by comparing the root mean square errors, as well as the correlation coefficient, R^2 [43]. Of the linearized Langmuir models, the second linear form appears to fit the data best, based on its RMSE and R^2, which appear to be better than those resulting from the NLLS fit. However, it is obvious from Figure 4.28 that the second linear form does not represent the observed data well. Figure 4.28 shows Langmuir isotherms resulting from the parameter estimates obtained from the linearized forms of the Langmuir equation. For comparison, the resulting RMSE and R^2 from the transformations of the linearized equations are calculated and compared to the RMSE and R^2 of the linear fits in Table 4.14. When considering these values, the second linear Langmuir form no longer appears to fit the data well. One reason for this discrepancy could be the change in weights and error distributions resulting from the linearizations, which are aspects of the model fit that are not captured in the R^2 and RMSE statistics [43]. Thus, the nonlinear models will be used for comparison, as they give more reliable parameter estimates [43].

Langmuir and Freundlich isotherms for europium sorption on flake (C) and powder (D) chitosan are shown in Figure 4.28. From visual inspection and comparison of the RMSE and R^2 of both models, it appears that both models provide a reasonable fit, with a slightly better fit provided by the Freundlich isotherm, as evidenced by the lower RMSE. In the case of uranyl sorption on powder chitosan (Figure 4.31 and Table 4.16), the Freundlich isotherm provides a superior fit, as well as resulting in statistically significant parameter estimates. For cobalt sorption on flake chitosan (C), the isotherms again provide approximately equivalent fits (Figure 4.30 and Table 4.15), and neither fit the data particularly well. This is likely a result of the data, as it contains points that may be considered outliers. Overall, it appears that the Freundlich isotherm better describes cation sorption onto chitosan for the cations investigated.

The isotherm for cobalt was performed for 1 hour and 168 hour contact times, in

order to evaluate the sensitivity of the model parameters on the contact time. Sorption isotherms are usually determined at equilibrium sorption time. In this work, except for cobalt, sorption isotherms were constructed instead from sorption data from 1 hour contact times. From the cobalt data (Table 4.15), it is observed, as expected, that the change in contact time has a large effect on the Langmuir maximum sorption parameter, q_m, and only a negligible effect on the Langmuir affinity constant K. Likewise, the Freundlich constant K is effected more than the parameter n.

The Langmuir separation factor, R_L, is commonly used to predict if an isotherm is favorable or unfavorable [14]:

$$R_L = \frac{1}{1 + KC_0} \tag{4.2}$$

where K is the Langmuir constant (L/mg) and C_0 is the initial metal concentration (mg/L). The value of R_L indicates if sorption is favorable ($0 < R_L < 1$), unfavorable ($R_L > 1$), linear ($R = 1$) or irreversible ($R_L = 0$). R_L is calculated for a range of C_0 for the Langmuir isotherm parameters for cobalt, europium and urnayl, as shown in Figure 4.32. It is observed that R_L is between zero and one for all initial metal concentrations between 0 and 1,000 mg/L for all metals, indicating the sorption is favorable. Present results are consistent with the results of Humelnicu et al. and Wang et al. for UO_2^{2+} sorption onto cross-linked chitosan ($R_L = 0.24$ with [UO_2^{2+}] = 20 mg/L [32]; R_L = 0.04 with [UO_2^{2+}] = 19 mg/L [92]; R_L = 0.06 with [UO_2^{2+}] = 20 mg/L, this work).

Table 4.12: Linear forms of the Langmuir and Freundlich isotherms.

Isotherm	Nonlinear form	Linear form	Plot
Langmuir	$q_e = \frac{q_m K C_e}{1+KC_e}$	$\frac{C_e}{q_e} = \frac{C_e}{q_m} + \frac{1}{q_m K_L}$	$\frac{C_e}{q_e}$ vs. C_e
		$\frac{1}{q_e} = \frac{1}{q_m K_L C_e} + \frac{1}{q_m}$	$\frac{1}{q_e}$ vs. $\frac{1}{C_e}$
		$q_e = q_m - \frac{q_e}{K_L C_e}$	q_e vs. $\frac{q_e}{q_m C_e}$
		$\frac{q_e}{C_e} = q_m K - q_m q_e$	$\frac{q_e}{C_e}$ vs. q_e
Freundlich	$q_e = K_F C_e^{1/n}$	$\log q_e = \log K_F + \frac{1}{n} \log C_e$	$\log q_e$ vs. $\log C_e$

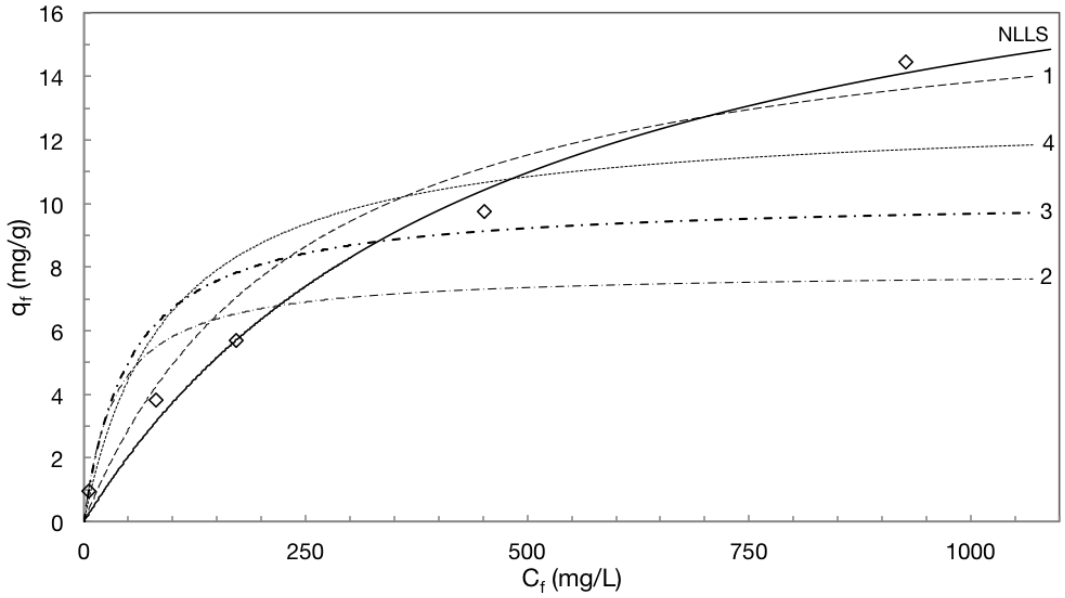

Figure 4.28: Langmuir isotherm, fit by NLLS and linearizations 1–4, for Eu(III) adsorption by chitosan C, with 5 g/L chitosan and Eu(III) concentration 10–1000 mg/L. Results are similar for other chitosan types.

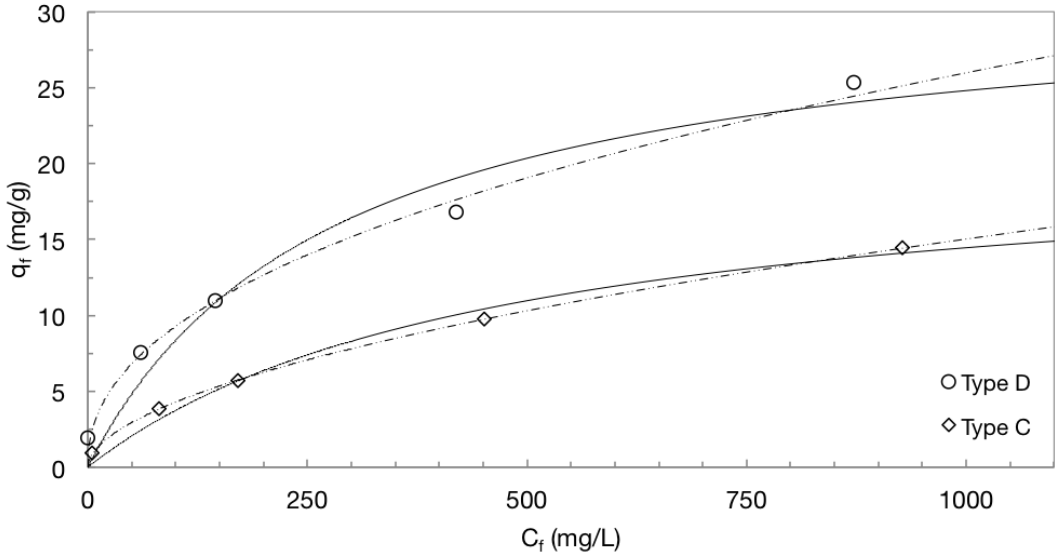

Figure 4.29: Langmuir (solid) and Freundlich (dashed) isotherms, fit by NLLS, for Eu(III) adsorption by chitosan C and D, with 5 g/L chitosan and Eu(III) concentration 10–1000 mg/L.

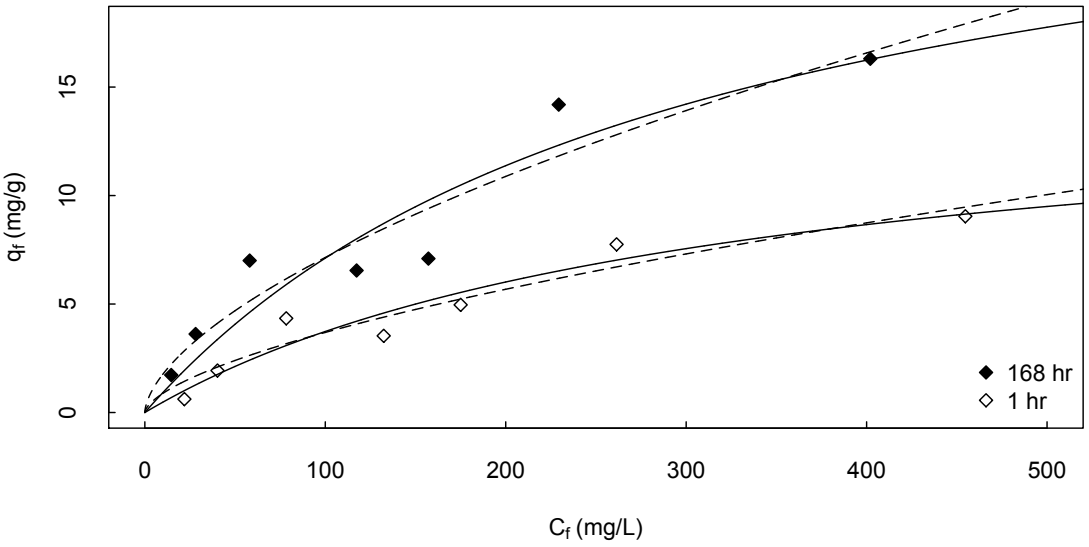

Figure 4.30: Langmuir (solid) and Freundlich (dashed) isotherms, fit by NLLS, for Co(II) sorption by chitosan C, with chitosan concentration 5 g/L, Co(II) concentration 25–500 mg/L, initial pH = 6.0 and 1 or 168 hour contact time.

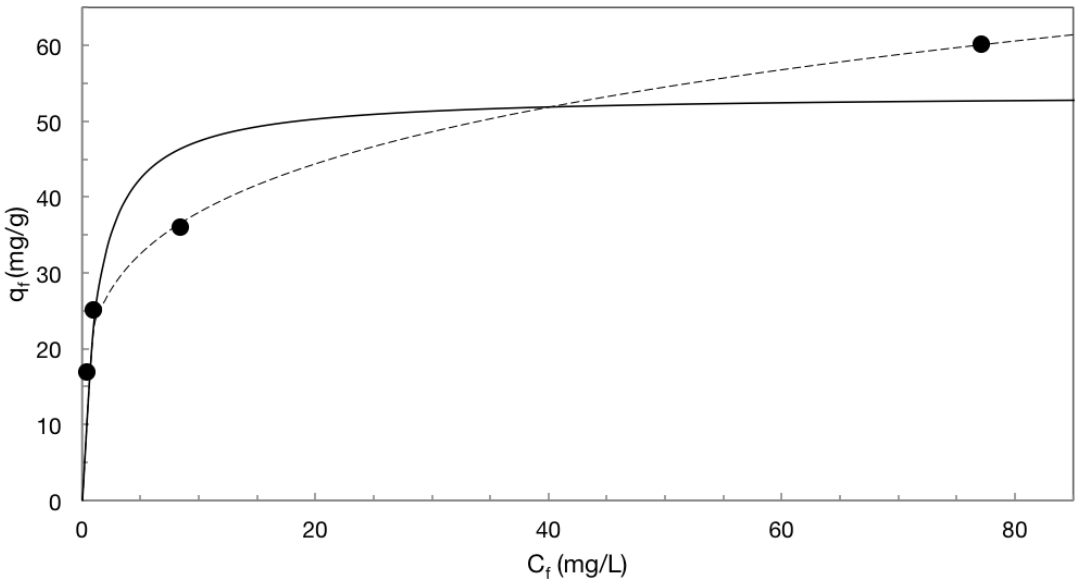

Figure 4.31: Langmuir (solid) and Freundlich (dashed) isotherms, fit by NLLS, for UO_2^{2+} sorption by chitosan D, with UO_2^{2+} concentration 200 mg/L and chitosan concentration 2 – 15 g/L, inital pH = 4.6 and 1 hour contact time.

Table 4.13: Isotherm model parameters for europium uptake by chitosan (type C, D) at initial pH = 5. RMSE and R^2 for linear models are for the linear fit.

Chitosan	Model		q_m (mg/g)	K	n	R^2	RMSE
C	Langmuir	Nonlinear	21.20	0.0021		0.99	0.73
		Linear 1	17.24	0.0040		0.91	7.7
		Linear 2	7.88	0.0282		0.98	0.06
		Linear 3	10.18	0.0194		0.55	4.08
		Linear 4	12.88	0.0106		0.55	0.06
	Freundlich	Nonlinear		0.349	1.84	0.99	0.08
		Linear		0.414	1.94	0.99	0.017
D	Langmuir	Nonlinear	31.76	0.0036		0.96	2.15
		Linear 1	27.39	0.0069		0.92	4.47
		Linear 2	12.53	0.57		0.97	0.04
		Linear 3	15.33	0.44		0.45	7.70
		Linear 4	18.85	0.20		0.45	2.28
	Freundlich	Nonlinear		1.20	2.19	0.99	0.98
		Linear		2.55	3.21	0.98	0.08

Table 4.14: Comparison of goodness-of-fit metrics for linearized isotherms and transformed linearized europium isotherms for chitosan (type C).

Model		Linear		Transformed	
		R^2	RMSE	R^2	RMSE
Langmuir	Nonlinear			0.99	0.73
	Linear 1	0.91	7.7	0.97	1.3
	Linear 2	0.98	0.06	0.65	4.3
	Linear 3	0.55	4.08	0.79	3.3
	Linear 4	0.55	0.06	0.88	2.6
Freundlich	Nonlinear			0.99	0.08
	Linear	0.99	0.29	0.99	0.28

Table 4.15: Isotherm model parameters, estimated by NLLS, for cobalt uptake by flake (C) chitosan. Conditions: 5 g/L chitosan, initial pH=6, initial [Co] varied 25–500 mg/L.

Model		q_m (mg/g)	K	n	R^2	RMSE
Langmuir	1 hr	15.5 ($\circ$)	0.0032 ($*$)		0.93	0.86
	168 hr	28.4	0.0033 ($*$)		0.88	2.00
Freundlich	1 hr		0.211	0.622 ($*$)	0.92	0.91
	168 hr		0.437	0.607 ($*$)	0.90	1.82

($*$) indicates the parameter estimate is statistically significant with $p < 0.05$.
($\circ$) indicates the parameter estimate is statistically significant with $0.05 < p < 0.1$.

Table 4.16: Isotherm model parameters, estimated by NLLS, for uranyl uptake by powder (D) chitosan. Conditions: initial pH=4.6, [UO_2^{2+}] = 200 mg/L, chitosan concentration 2 – 15 g/L, and 1 hour contact time.

Model	q_m (mg/g)	K	n	R^2	RMSE
Langmuir	53.6 ($*$)	0.761		0.83	9.4
Freundlich		22.63 ($*$)	0.225 ($*$)	0.99	2.3

($*$) indicates the parameter estimate is statistically significant with $p < 0.05$.

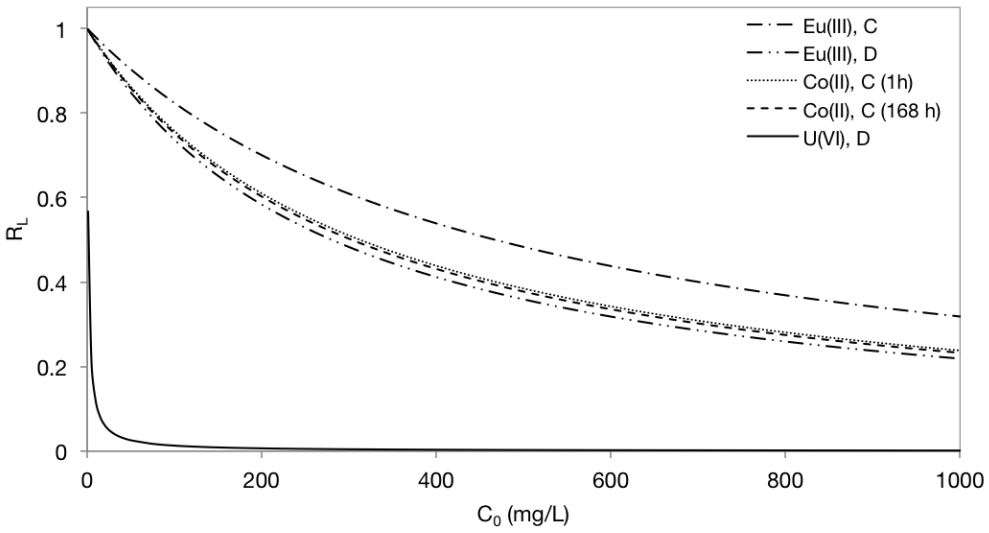

Figure 4.32: Langmuir separation factor, R_L, as a function of initial metal concentration, C_0 for sorption of Co(II), Eu(III) and U(VI) on chitosan (C and D).

5 Conclusions and Future Work

This study has shown that chitosan may be an effective sorbent for Co(II), Eu(III) and U(VI) under appropriate conditions. The sorption isotherms and kinetics have been modeled under these conditions.

The Freundlich isotherm was found to fit the experimental data well for Co(II), Eu(III) and U(VI), with the adsorption capacity of the cations following Co < Eu < U. The Langmuir isotherm was also found to fit the data reasonably. Both isotherm models were found to be sensitive to the method of parameter estimation, with the non-linear least squares method selected as giving the best parameter estimates.

The study also found that the size of the chitosan particle affects the sorption capacity as well as the sorption kinetics. Other conditions, such as pre-hydration of the polymer and stirring conditions were found to effect uranyl sorption capacity and kinetics.

The sorption kinetics were modeled by the intraparticle diffusion, pseudo-first order, pseudo-second order, and Elovich models. Parameter estimates were found to be sensitive to the method used (ordinary linear vs. non-linear least squares regression), as with isotherm modeling. Multiple linear sections were observed for each sorbent-metal system in the intraparticle diffusion model, suggesting a change in sorption mechanism with time. The results of this model also indicated the existence of a film boundary layer around the sorbent particles which may also contribute to the limiting step. As found with many biosorption systems, reasonable fit was attained with the pseudo-second order model.

Future work, to determine the performance of chitosan sorbents toward these metals and others under additional conditions will provide additional insight toward the possibility of using such sorbents to effectively treat the aqueous waste streams resulting from the nuclear technologies. Further work to determine the effect of ionic strength, other metal ions in solution, and presence of ligands or organic contaminants on the sorption capacity of chitosan will be necessary before the sorbent can be determined appropriate for use in such conditions. Additional work to determine the

ability to desorb metals from chitosan will not only determine if the sorbent can be reused, but will also provide insight into the strength and stability of the chitosan-metal complex.

Research into methods to effectively and efficiently treat radioactive waste to adequately reduce volume and activity, as well as minimize environmental mobility, prior to permanent disposal is complex and ongoing. Capturing radionuclides from high-volume, low concentration aqueous waste streams on an easily disposed or reusable sorbent represents one avenue toward this goal.

References

[1] Akkaya, R.; Ulusoy, U. Adsorptive features of chitosan entrapped in polyacrylamide hydrogel for Pb^{2+}, UO_2^{2+}, and Th^{4+}. *Journal of Hazardous Materials* **2008**, *151*, 380–8.

[2] Aranaz, I.; Mengíbar, M.; Harris, R.; Paños, I.; Miralles, B.; Acosta, N.; Galed, G.; Heras, A. Functional characterization of chitin and chitosan. *Current Chemical Biology* **2009**, *3*, 203–230.

[3] Areco, M. M.; dos Santos Afonso, M.; Valdman, E. Zinc biosorption by seaweed illustrated by the zincon colorimetric method and the Langmuir isotherm. *Journal of Chemical Education* **2007**, *84*, 302.

[4] Baes, C. F.; Mesmer, R. E. *The Hydrolysis of Cations*, First Ed; Wiley: New York, 1976.

[5] Balázs, N.; Sipos, P. Limitations of pH-potentiometric titration for the determination of the degree of deacetylation of chitosan. *Carbohydrate Research* **2007**, *342*, 124–30.

[6] Bassi, R. Removal of selected metal ions from aqueous solutions using chitosan flakes. *Separation Science and Technology* **2000**, *35*, 547–560.

[7] Baxter, A.; Dillon, M.; Taylor, K. A.; Roberts, G. A. Improved method for i.r. determination of the degree of N-acetylation of chitosan. *International Journal of Biological Macromolecules* **1992**, *14*, 166–169.

[8] Bhatnagar, A.; Sillanpää, M. Applications of chitin- and chitosan-derivatives for the detoxification of water and wastewater– a short review. *Advances in Colloid and Interface Science* **2009**, *152*, 26–38.

[9] Bhatnagar, A.; Sillanpää, M. A review of emerging adsorbents for nitrate removal from water. *Chemical Engineering Journal* **2011**, *168*, 493–504.

[10] Camci-Unal, G.; Pohl, N. L. B. Quantitative determination of heavy metal contaminant complexation by the carbohydrate polymer chitin. *Journal of Chemical & Engineering Data* **2010**, *55*, 1117–1121.

[11] Cárdenas, G.; Anaya, P.; Plessing, C. von; Rojas, C.; Sepúlveda, J. Chitosan composite films. Biomedical applications. *Journal of Materials Science: Materials in Medicine* **2008**, *19*, 2397–2405.

[12] Chatterjee, S.; Woo, S. H. The removal of nitrate from aqueous solutions by chitosan hydrogel beads. *Journal of Hazardous Materials* **2009**, *164*, 1012–1018.

[13] Chojnacka, K. Biosorption and bioaccumulation–the prospects for practical applications. *Environment International* **2010**, *36*, 299–307.

[14] Dahiya, S.; Tripathi, R. M.; Hegde, a. G. Biosorption of heavy metals and radionuclide from aqueous solutions by pre-treated arca shell biomass. *Journal of Hazardous Materials* **2008**, *150*, 376–386.

[15] Dambies, L Characterization of metal ion interactions with chitosan by X-ray photoelectron spectroscopy. *Colloids and Surfaces A: Physicochemical and Engineering Aspects* **2000**, *177*, 203–214.

[16] Drace, Z New Developments and Improvements in Processing of 'Problematic' Radioactive Waste.; tech. rep. December; International Atomic Energy Agency: Vienna, 2007.

[17] Dzul Erosa, M.; Saucedo Medina, T.; Navarro Mendoza, R.; Avila Rodriguez, M.; Guibal, E. Cadmium sorption on chitosan sorbents: kinetic and equilibrium studies. *Hydrometallurgy* **2001**, *61*, 157–167.

[18] El-Khaiary, M. I.; Malash, G. F.; Ho, Y.-S. On the use of linearized pseudo-second-order kinetic equations for modeling adsorption systems. *Desalination* **2010**, *257*, 93–101.

[19] Evans, J. R.; Davids, W. G.; MacRae, J. D.; Amirbahman, A. Kinetics of cadmium uptake by chitosan-based crab shells. *Water research* **2002**, *36*, 3219–3226.

[20] Gadd, G. M. Biosorption: critical review of scientific rationale, environmental importance and significance for pollution treatment. *Journal of Chemical Technology and Biotechnology* **2009**, *84*, 13–28.

[21] Guibal, E. Interactions of metal ions with chitosan-based sorbents: a review. *Separation and Purification Technology* **2004**, *38*, 43–74.

[22] Guibal, E.; Milot, C; Tobin, J. M. Metal-anion sorption by chitosan beads: equilibrium and kinetic studies. *Industrial & Engineering Chemistry Research* **1998**, *37*, 1454–1463.

[23] Guibal, E.; Touraud, E.; Roussy, J. Chitosan interactions with metal Iins and dyes: dissolved-state vs. solid-state application. *World Journal of Microbiology and Biotechnology* **2005**, *21*, 913–920.

[24] Guibal, E.; Jansson-Charrier, M.; Saucedo, I.; Cloirec, P. L. Enhancement of metal ion sorption performances of chitosan: effect of the structure on the diffusion properties. *Langmuir* **1995**, *11*, 591–598.

[25] Guzmán, J.; Saucedo, I.; Navarro, R.; Revilla, J.; Guibal, E. Vanadium interactions with chitosan: influence of polymer protonation and metal speciation. *Langmuir* **2002**, *18*, 1567–1573.

[26] Gyliene, O; Nivinskiene, O; Vengris, T Sorption of tartrate, citrate, and EDTA onto chitosan and its regeneration applying electrolysis. *Carbohydrate Research* **2008**, *343*, 1324–1332.

[27] Hayes, K.; Papelis, C; Leckie, J. Modeling ionic strength effects on anion adsorption at hydrous oxide/solution interfaces. *Journal of Colloid and Interface Science* **1988**, *125*, 717–726.

[28] Ho, Y. S.; Ng, J. C.; McKay, G. Kinetics of pollutant sorption by biosorbents: review. *Separation and Purification Reviews* **2000**, *29*, 189–232.

[29] Ho, Y.-S. Second-order kinetic model for the sorption of cadmium onto tree fern: a comparison of linear and non-linear methods. *Water Research* **2006**, *40*, 119–125.

[30] Hsien, T.; Rorrer, G. L. Effects of acylation and cross-linking on the material properties and cadmium ion adsorption capacity of porous chitosan beads. *Separation Science and Technology* **1995**, *30*, 2455–2475.

[31] Hsien, T.; Rorrer, G. L. Heterogeneous cross-linking of chitosan gel beads: kinetics, modeling, and influence on cadmium ion adsorption capacity. *Industrial and Engineering Chemistry Research* **1997**, *36*, 3631–3638.

[32] Humelnicu, D.; Dinu, M. V.; Dragan, E. S. Adsorption characteristics of UO(2)(2+) and Th(4+) ions from simulated radioactive solutions onto chitosan/clinoptilolite sorbents. *Journal of Hazardous Materials* **2011**, *185*, 447–455.

[33] Inoue, K.; Yoshizuka, K.; Ohto, K. Adsorptive separation of some metal ions by complexing agent types of chemically modified chitosan. *Analytica Chimica Acta* **1999**, *388*, 209–218.

[34] Ishikawa, S.-i.; Suyama, K.; Arihara, K.; Itoh, M. Selective recovery of uranium and thorium ions from dilute aqueous solutions by animal biopolymers. *Biological Trace Element Research* **2002**, *86*, 227–36.

[35] Ishikawa, S.; Suyama, K Biosorption of actinides from dilute waste actinide solution by egg-shell membrane. *Applied Biochemistry and Biotechnology* **1999**, *77*, 521–533.

[36] Jansson-Charrier, M.; Guibal, E.; Roussy, J.; Delanghe, B.; Le Cloirec, P Vanadium (IV) sorption by chitosan: kinetics and equilibrium. *Water Research* **1996**, *30*, 465–475.

[37] Jaworska, M.; Sakurai, K.; Gaudon, P.; Guibal, E. Influence of chitosan characteristics on polymer properties. I: crystallographic properties. *Polymer International* **2003**, *52*, 198–205.

[38] Jiang, X.; Chen, L. A new linear potentiometric titration method for the determination of deacetylation degree of chitosan. *Carbohydrate Polymers* **2003**, *54*, 457–463.

[39] Kasaai, M. R. Determination of the degree of N-acetylation for chitin and chitosan by various NMR spectroscopy techniques: a review. *Carbohydrate Polymers* **2010**, *79*, 801–810.

[40] Khambhaty, Y.; Mody, K.; Basha, S.; Jha, B. Pseudo-second-order kinetic models for the sorption of Hg(II) onto dead biomass of marine Aspergillus niger: comparison of linear and non-linear methods. *Colloids and Surfaces A: Physicochemical and Engineering Aspects* **2008**, *328*, 40–43.

[41] Khan, T. A.; Peh, K. K.; Ch'ng, H. S. Reporting degree of deacetylation values of chitosan: the influence of analytical methods. *Journal of Pharmacy and Pharmaceutical Sciences* **2002**, *5*, 205–212.

[42] Kim, E.; Benedetti, M. F.; Boulègue, J. Removal of dissolved rhenium by sorption onto organic polymers: study of rhenium as an analogue of radioactive technetium. *Water Research* **2004**, *38*, 448–454.

[43] Kinniburgh, D. G. General purpose adsorption isotherms. *Environmental Science and Technology* **1986**, *20*, 895–904.

[44] Kumar, K. V. Linear and non-linear regression analysis for the sorption kinetics of methylene blue onto activated carbon. *Journal of Hazardous Materials* **2006**, *137*, 1538–1544.

[45] Kumar, K. V.; Sivanesan, S. Selection of optimum sorption kinetics: comparison of linear and non-linear method. *Journal of Hazardous Materials* **2006**, *B134*, 277–279.

[46] Langmuir, I. The adsorption of gases on plane surfaces of glass, mica and platinum. *Journal of the American Chemical Society* **1918**, *40*, 1361–1403.

[47] Lavertu, M.; Xia, Z.; Serreqi, A. N.; Berrada, M.; Rodrigues, A.; Wang, D.; Buschmann, M.; Gupta, A. A validated 1H NMR method for the determination of the degree of deacetylation of chitosan. *Journal of Pharmaceutical and Biomedical Analysis* **2003**, *32*, 1149–1158.

[48] Levitskaia, T. G.; Chen, Y.; Fulton, J. L.; Sinkov, S. I. Neodymium(III) complexation by amino-carbohydrates via a ligand-controlled hydrolysis mechanism. *Chemical Communications* **2011**, *47*, 8160–8162.

[49] Li, C. B.; Hein, S.; Wang, K. Biosorption of chitin and chitosan. *Materials Science and Technology* **2008**, *24*, 1088–1099.

[50] Limousin, G; Gaudet, J; Charlet, L; Szenknect, S; Barthes, V; Krimissa, M Sorption isotherms: a review on physical bases, modeling and measurement. *Applied Geochemistry* **2007**, *22*, 249–275.

[51] McKay, G.; Blair, H.; Findon, A In *Immobilisation of Ions by Bio-Sorption*, First Ed; Eccles, H, Hunt, S, Eds.; Ellis Horwood: Chichester, 1989; Chapter 2, pp 59–69.

[52] Mckay, G.; Blair, H.; Findon, A. Equilibrium studies for the sorption of metal ions onto chitosan. *Indian Journal of Chemistry* **1989**, *28A*, 356–360.

[53] Mizera, J; Mizerová, G; Machovic, V; Borecká, L Sorption of cesium, cobalt and europium on low-rank coal and chitosan. *Water Research* **2007**, *41*, 620–626.

[54] Muzzarelli, R. A. A. *Chitin*, First Ed.; Pergamon Press: Oxford, 1977.

[55] Navarro, R.; Guzmán, J.; Saucedo, I.; Revilla, J.; Guibal, E. Recovery of metal ions by chitosan: sorption mechanisms and influence of metal speciation. *Macromolecular Bioscience* **2003**, *3*, 552–561.

[56] Ng, J.; Cheung, W.; McKay, G. Equilibrium studies of the sorption of Cu(II) ions onto chitosan. *Journal of Colloid and Interface Science* **2002**, *255*, 64–74.

[57] Nishi, N.; Maekita, Y.; Nishimura, S.; Hasegawa, O.; Tokura, S. Highly phosphorylated derivatives of chitin, partially deacetylated chitin and chitosan as new functional polymers: metal binding property of the insolubilized materials. *International Journal of Biological Macromolecules* **1987**, *9*, 109–114.

[58] Ogawa, K. In *Material Science of Chitin and Chitosan*, First Ed; Uragami, T., Tokura, S., Eds.; Springer, 2006; Chapter 2, pp 21–49.

[59] Ogawa, K.; Oka, K. X-ray study of chitosan-transition metal complexes. *Chemistry of Materials* **1993**, *5*, 726–728.

[60] Onsoyen, E.; Skaugrud, O. Metal recovery using chitosan. *Journal of Chemical Technology and Biotechnology* **1990**, *49*, 395–404.

[61] Park, J.; Park, M.; Park, K. Mechanism of metal ion binding to chitosan in solution, cooperative inter-and intramolecular chelations. *Bulletin of the Korean Chemical Society* **1984**, *5*, 108–112.

[62] Park, S.; Marsh, K.; Rhim, J. Characteristics of different molecular weight chitosan films affected by the type of organic solvents. *Journal of Food Science* **2002**, *67*, 194–197.

[63] Pillai, C.; Paul, W.; Sharma, C. P. Chitin and chitosan polymers: Chemistry, solubility and fiber formation. *Progress in Polymer Science* **2009**, *34*, 641–678.

[64] Piron, E.; Accominotti, M.; Domard, A. Interaction between chitosan and uranyl ions. Role of physical and physicochemical parameters on the kinetics of sorption. *Langmuir* **1997**, *13*, 1653–1658.

[65] Piron, E.; Domard, A. Interaction between chitosan and uranyl ions. Part 1. Role of physicochemical parameters. *International Journal of Biological Macromolecules* **1997**, *21*, 327–335.

[66] Piron, E.; Domard, A. Formation of a ternary complex between chitosan and ion pairs of strontium carbonate. *International Journal of Biological Macromolecules* **1998**, *23*, 113–120.

[67] Piron, E.; Domard, A. Interaction between chitosan and uranyl ions. Part 2. Mechanism of interaction. *International Journal of Biological Macromolecules* **1998**, *22*, 33–40.

[68] Plazinski, W.; Rudzinski, W.; Plazinska, A. Theoretical models of sorption kinetics including a surface reaction mechanism: a review. *Advances in Colloid and Interface Science* **2009**, *152*, 2–13.

[69] Puigdomenech, I. Hydra/Medusa Chemical Equilibrium Database and Plotting Software.; Royal Institute of Technology: Stockholm, Sweden, 2011, http://www.kemi.kth.se/utbildning/gk/kemiskjmv/.

[70] R Development Core Team R: A Language and Environment for Statistical Computing., ISBN 3-900051-07-0; R Foundation for Statistical Computing: Vienna, Austria, 2011, http://www.R-project.org.

[71] Rathke, T.; Hudson, S. Determination of the degree of N-deacetylation in chitin and chitosan as well as their monomer sugar ratios by near infrared spectroscopy. *Journal of Polymer Science Part A: Polymer Chemistry* **1993**, *31*, 749–753.

[72] Ravi Kumar, M A review of chitin and chitosan applications. *Reactive and Functional Polymers* **2000**, *46*, 1–27.

[73] Rhazi, M Contribution to the study of the complexation of copper by chitosan and oligomers. *Polymer* **2002**, *43*, 1267–1276.

[74] Rhazi, M; Desbrueres, J; Tolaimate, A; Rinaudo, M; Vottero, P; Alagui, A; El Meray, M Influence of the nature of the metal ions on the complexation with chitosan: Application to the treatment of liquid waste. *European Polymer Journal* **2002**, *28*, 1523–1530.

[75] Rinaudo, M Chitin and chitosan: Properties and applications. *Progress in Polymer Science* **2006**, *31*, 603–632.

[76] Riordan, C; Bustard, M; Putt, R; McHale, A. P. Removal of uranium from solution using residual brewery yeast: combined biosorption and precipitation. *Biotechnology Letters* **1997**, *19*, 385–387.

[77] Sabnis, S.; Block, L. H. Improved infrared spectroscopic method for the analysis of degree of N-deacetylation of chitosan. *Polymer Bulletin* **1997**, *39*, 67–71.

[78] Sakaguchi, T.; Horikoshi, T.; Nakajima, A. Adsorption of uranium by chitin phosphate and chitosan phosphate. *Agricultural and Biological Chemistry* **1981**, *45*, 2191–2195.

[79] Schatz, C.; Viton, C.; Delair, T.; Pichot, C.; Domard, A. Typical physicochemical behaviors of chitosan in aqueous solution. *Biomacromolecules* **2003**, *4*, 641–648.

[80] Shamov, M. V.; Bratskaya, S. Y.; Avramenko, V. a. Interaction of carboxylic acids with chitosan: effect of pK and hydrocarbon chain length. *Journal of Colloid and Interface Science* **2002**, *249*, 316–321.

[81] Shigemasa, Y; Matsuura, H; Sashiwa, H; Saimoto, H Evaluation of different absorbance ratios from infrared spectroscopy for analyzing the degree of deacetylation in chitin. *International Journal of Biological Macromolecules* **1996**, *18*, 237–242.

[82] Sicupira, D.; Campos, K.; Vincent, T.; Leao, V.; Guibal, E. Palladium and platinum sorption using chitosan-based hydrogels. *Adsorption* **2010**, 127–139.

[83] Skopp, J. Derivation of the Freundlich adsorption isotherm from kinetics. *Journal of Chemical Education* **2009**, *86*, 1341–1343.

[84] Sorlier, P; Denuzière, A; Viton, C; Domard, A. Relation between the degree of acetylation and the electrostatic properties of chitin and chitosan. *Biomacromolecules* **2001**, *2*, 765–772.

[85] Tan, S. C.; Khor, E; Tan, T. K.; Wong, S. M. The degree of deacetylation of chitosan: advocating the first derivative UV-spectrophotometry method of determination. *Talanta* **1998**, *45*, 713–719.

[86] Trung, T. S.; Ng, C.-H.; Stevens, W. F. Characterization of decrystallized chitosan and its application in biosorption of textile dyes. *Biotechnology Letters* **2003**, *25*, 1185–1190.

[87] Tsezos, M In *Immobilisation of Ions by Bio-Sorption*, First Ed; Eccles, H, Hunt, S, Eds.; Ellis Horwood: Chichester, 1986; Chapter 5, pp 201–218.

[88] Valenta, C.; Christen, B.; Bernkop-Schnürch, A. Chitosan-EDTA conjugate: a novel polymer for topical gels. *The Journal of Pharmacy and Pharmacology* **1998**, *50*, 445–452.

[89] Varma, A.; Deshpande, S.; Kennedy, J. Metal complexation by chitosan and its derivatives: a review. *Carbohydrate Polymers* **2004**, *55*, 77–93.

[90] Verbych, S.; Bryk, M.; Chornokur, G.; Fuhr, B. Removal of copper(II) from aqueous solutions by chitosan adsorption. *Separation Science and Technology* **2005**, *40*, 1749–1759.

[91] Volesky, B.; Holan, Z. R. Biosorption of heavy metals. *Biotechnology Progress* **1995**, *11*, 235–50.

[92] Wang, G.; Liu, J.; Wang, X.; Xie, Z.; Deng, N. Adsorption of uranium(VI) from aqueous solution onto cross-linked chitosan. *Journal of Hazardous Materials* **2009**, *168*, 1053–1058.

[93] Wong, Y.; Szeto, Y.; Cheung, W.; McKay, G. Adsorption of acid dyes on chitosan – equilibrium isotherm analyses. *Process Biochemistry* **2004**, *39*, 695–704.

[94] Yu, Q.; Kandegedara, A.; Xu, Y.; Rorabacher, D. B. Avoiding interferences from Good's buffers: a contiguous series of noncomplexing tertiary amine buffers covering the entire range of pH 3-11. *Analytical Biochemistry* **1997**, *253*, 50–56.

[95] Zhang, C.; Jia, Z. Preparation of porous chitosan microsphere absorbent and research on Its absorption ability for Cu2+ and Zn2+. *International Journal of Chemistry* **2010**, *2*, 113–120.

[96] Zhang, H; Neau, S. H. In vitro degradation of chitosan by a commercial enzyme preparation: effect of molecular weight and degree of deacetylation. *Biomaterials* **2001**, *22*, 1653–1658.